

# Intraseasonal to interannual variability of zooplankton biomass and standing stock inferred from ADCP backscatter in the eastern Arabian Sea

Ranjan Kumar Sahu<sup>a,b</sup>, D. Shankar<sup>a,b,\*</sup>, P. Amol<sup>b,c</sup>, S. G. Aparna<sup>a,b</sup>,  
D. V. Desai<sup>a,b</sup>

<sup>a</sup>*CSIR-National Institute of Oceanography, Dona Paula, 403004, Goa, India*

<sup>b</sup>*Academy of Scientific and Innovative Research (AcSIR), Ghaziabad, 201002,  
Uttar Pradesh, India*

<sup>c</sup>*CSIR-NIO Regional Centre, Visakhapatnam, 530017, Andhra Pradesh, India*

---

## Abstract

We analyse the variability of zooplankton biomass and standing stock (ZSS: integral of biomass over 24–120 m) at timescales ranging from intraseasonal to interannual using biomass data derived from seven ADCP (acoustic Doppler current profiler) moorings deployed on the continental slope in the eastern Arabian Sea (EAS) during 2017–2023. The biomass time series confirms the expected decay in biomass with depth. The monthly climatology of ZSS has its minimum (maximum) during the summer (winter) monsoon. The asymmetry reflected in the rapid rise (slow fall) in biomass following the minimum (maximum) leads to significant intra-annual (100–250 days) variability within the seasonal cycle. The annual cycle (300–400 days) dominates in the northeastern AS, but intra-annual and intraseasonal (5–90 days) variability dominate in the southeastern AS. The intraseasonal range of biomass is comparable to or exceeds the seasonal range, but ZSS does not show comparable intraseasonal variability because the deviation from the mean can be

---

\*Corresponding author  
Email address: [shankar@nio.res.in](mailto:shankar@nio.res.in) (D. Shankar)

in opposite directions in the upper and lower parts of the top  $\sim$ 140 m. Also evident are spikes that last a day or more and often exceed two standard deviations from the mean. The seasonal cycle and intraseasonal variability are not related to the variation of satellite chl-*a*, suggesting a significant role for the microbial loop and plankton not captured in satellite data. The strong intraseasonal variability calls into question biomass and ZSS contours based on traditional ship-based sampling.

*Keywords:* ADCP backscatter, moorings, zooplankton sampling, multiple plankton net, intraseasonal variability, Indian Ocean.

---

## 1. Introduction

### 2 1.1. Background

Zooplankton play a vital role in the pelagic ecosystem by enabling the  
4 hierarchical transport of organic matter from primary producers to higher  
trophic levels, thereby impacting the fish population (Ohman and Hirche,  
6 2001) and the carbon pump of the deep ocean (Quéré et al., 2016). Owing  
to their diel vertical migration (DVM), they probably constitute the largest  
8 migrating organism in terms of biomass (Hays, 2003). Zooplankton depend  
not only on phytoplankton, but also on the microbial loop (Azam et al.,  
10 1983); the zooplankton abundance or standing stock therefore depends on  
environmental variables (e. g., mixed-layer depth or MLD, insolation, oxy-  
12 gen, thermocline, nutrient availability, Chlorophyll-*a* (chl-*a*) concentration,  
and daily primary production). As is true of the rest of the world ocean, the  
14 biological productivity of the north Indian Ocean (NIO; north of 5°N in the  
Indian Ocean) is essentially driven by the physics and chemistry (see, for  
16 example, Subrahmanyam, 1959; Ryther et al., 1966; Banse, 1968; Nair, 1970;  
Qasim, 1977; Banse, 1995; Lévy et al., 2007; McCreary et al., 2009; Vijith  
18 et al., 2016; Shankar et al., 2016, 2019; Amol et al., 2020), with changing dy-  
namical conditions leading to variations in physico-chemical properties and  
20 therefore causing blooms and growth of plankton in favourable conditions.  
The changes are strongly influenced by the seasonal cycle in the NIO (Banse,  
22 1968; McCreary et al., 1996, 2009; Lévy et al., 2007; Shankar et al., 2019;  
Aparna et al., 2022). The eastern boundary of the Arabian Sea contains  
24 the West India Coastal Current (WICC), which reverses seasonally, flow-  
ing poleward (equatorward) during November–February (June–September)  
26 (Banse, 1968; Shetye et al., 1990, 1991; McCreary et al., 1993; Shankar and

Shetye, 1997; Shankar et al., 2002; Vijith et al., 2022).

A direct consequence of this reversal is the seasonal cycle of the thermocline (Shetye et al., 1990, 1991; Vijith et al., 2022) and oxycline (DeSousa et al., 1996; Schmidt et al., 2020) due to the upwelling (downwelling) favourable conditions during summer (winter) in the eastern Arabian Sea (EAS; Shetye et al., 1990, 1991; Vijith et al., 2022); the MLD responds to the changes in the thermocline and the mixing driven by the local winds and the changes in near-surface stratification (Shetye et al., 1991; Prasad and Bahulayan, 1996; Kumar and Narvekar, 2005). In response, the phytoplankton biomass and chl-*a* concentration changes with season (Subrahmanyam and Sarma, 1960; Banse, 1968; Kumar and Narvekar, 2005; Lévy et al., 2007; McCreary et al., 2009; Vijith et al., 2016; Shankar et al., 2019). Upwelling during the summer monsoon leads to maximum chl-*a* growth in the EAS (Banse, 1968; Banse and English, 2000; McCreary et al., 2009; Hood et al., 2017; Bemal et al., 2018; Shi and Wang, 2022). During the winter monsoon, convective mixing driven by dry winds was considered the key process leading to the deep mixed layer in the northeastern Arabian Sea (NEAS; Banse, 1968; Shetye et al., 1992; Madhupratap et al., 1996b; McCreary et al., 1996; Lévy et al., 2007), but recent results show that the poleward advection of warm and fresher water plays a key role in restricting the deep mixed layers to the northern part of the NEAS (Shankar et al., 2016). This deepening of the mixed layer leads to a winter chl-*a* peak in the NEAS (Madhupratap et al., 1996b; McCreary et al., 1996; Lévy et al., 2007; Vijith et al., 2016; Shankar et al., 2016; Keerthi et al., 2017; Shi and Wang, 2022). In the southeastern Arabian Sea (SEAS), downwelling Rossby waves modulate chl-*a* during the winter monsoon, but this effect is limited to the neighbourhood of the coast and islands (Amol et al., 2020); hence, the chl-*a*

54 peak in the SEAS is limited to the summer monsoon.

The zooplankton grazing peak is instantaneous with no time delay from  
55 peak phytoplankton production (Li et al., 2000; Barber et al., 2001), but its  
population growth lags (Rehim and Imran, 2012; Almén and Tamelander,  
56 2020) depending on its gestation period and other limiting aspects. Some  
studies suggest that the peak timing of zooplankton may not change in par-  
58 allel with phytoplankton blooms (Winder and Schindler, 2004), but others  
indicate that a lag exists between primary production and the transfer of en-  
60 ergy to higher trophic levels (Brock and McClain, 1992; Brock et al., 1991).  
Conventional, ship-based zooplankton sampling, by capturing only a few  
62 snapshots of the variation, provides an incoherent or incomplete description  
of the spatio-temporal variation of zooplankton (Ramamurthy, 1965; Mad-  
64 hupratap et al., 1992; Piontkovski et al., 1995; Madhupratap et al., 1996a;  
Wishner et al., 1998; Nair et al., 1999; Barber et al., 2001; Jyothibabu et al.,  
66 2010; Khandagale et al., 2022). Generating a time series of zooplankton  
biomass and standing stock is, however, possible with calibrated acoustic  
68 instruments such as the acoustic Doppler current profiler (ADCP) (Edvard-  
sen et al., 2003; Smith and Madhupratap, 2005; Smeti et al., 2015; Kang  
70 et al., 2024). The ADCP, by providing a continuous time series at a high  
72 temporal resolution, can reveal details of the complex interplay between the  
74 physico-chemical and ecosystem variables (Jiang et al., 2007; Potiris et al.,  
2018; Shankar et al., 2019; Aparna et al., 2022; Nie et al., 2023), and has  
76 been used to map zooplankton migration (Inoue et al., 2016; Ursella et al.,  
2018, 2021) and their seasonal to annual variation (Jiang et al., 2007; Hobbs  
78 et al., 2021; Liu et al., 2022; Aparna et al., 2022).

The relationship between ADCP backscatter and the abundance and  
80 size of zooplankton was described by Greenlaw (1979) with mono-frequency

backscatter used to estimate abundance along with knowledge of mean zooplankton size. The popularity of the ADCP as a tool to study temporal and spatial variation of zooplankton biomass increased in the 1990s following the introduction of high-frequency echo sounders (Flagg and Smith, 1989; Wiebe et al., 1990; Batchelder et al., 1995; Greene et al., 1998; Rippeth and Simpson, 1998). The ADCP backscatter has been used to study DVM and the spatial and temporal variability of zooplankton biomass in different marine regions, such as the southwestern Pacific (Smeti et al., 2015), the Lazarev Sea in Antarctica (Cisewski et al., 2010), the Canadian Arctic (Hamilton et al., 2013), and the Corsica Channel in the northwestern Mediterranean Sea (Guerra et al., 2019). Yet, in spite of the existence of moored-buoy networks deployed across the world ocean to measure currents, the potential of acoustics for understanding coupled physical and biological processes is poorly exploited (Davis et al., 2019; Shankar et al., 2019; Aparna et al., 2022). Aparna et al. (2022) (A22 hereafter) showed how the ADCP mooring network in the EAS (Amol et al., 2014; Chaudhuri et al., 2020) could be used to map the seasonal cycle of zooplankton biomass and standing stock, permitting an analysis of the physico-chemical forcing of their climatological seasonal variation.

### 100    1.2. Objectives and scope

The network of ADCPs used by A22 to map the seasonal cycle of zooplankton biomass and standing stock was originally deployed on the continental slope off the west coast of India to map the variability of the WICC on time scales ranging from the seasonal to the intraseasonal and to provide a measure of its interannual variability (Amol et al., 2014; Chaudhuri et al., 2020). A22 showed that the zooplankton peaks (and troughs) are influenced

by the seasonal movement of the thermocline, the oxygen minimum zone  
108 (OMZ), and the MLD. Their analysis showed that the zooplankton stand-  
ing stock (ZSS) tends to decrease in the SEAS during the summer monsoon,  
110 when upwelling facilitates an increase in phytoplankton biomass.

A22 used ADCP backscatter data from three moorings, one each located  
112 off Mumbai (NEAS), Goa (central-eastern Arabian Sea or CEAS), and Kol-  
lam (SEAS) for the period October 2012 to December 2020. We extend the  
114 work of A22 by presenting data from four additional moorings in the EAS  
and highlight the significant intraseasonal variability of biomass and ZSS  
116 revealed by the ADCP data. The article is organized as follows: data sets  
and methods employed are described in Section 2. Section 3 describes the  
118 observed time series and the climatology of zooplankton biomass and ZSS,  
and their seasonal cycle and variability. A brief discussion on interannual  
120 variability in Section 4 is followed by a detailed discussion in Section 5 on  
intraseasonal variability, which is a major focus in this study. Section 6  
122 summarises the results and discusses their implications.

## 2. Data and methods

In this section, we describe the data sets used in this article: the primary  
124 data consist of ADCP backscatter (Section 2.1) and zooplankton biomass  
126 (Section 2.2), along with additional supporting data sets (Section 2.3). A  
detailed description of the time series analysis methods—such as wavelet  
128 analysis (Torrence and Compo, 1998; Maraun and Kurths, 2004), imple-  
mented using the PyCWT module, and filtering using the Lanczos filter, is  
130 provided in supplementary Section XX.

### 2.1. The ADCP backscatter time series

132        The ADCP backscatter forms the primary data set used in this article.  
133        The four additional moorings include one off Kanyakumari (in the SEAS,  
134        south of Kollam and on the slope off the southern tip of the Indian main-  
135        land), Udupi (just north of the SEAS–CEAS boundary), Jaigarh (north of  
136        Goa in the CEAS), and Okha (north of Mumbai in the NEAS); all these  
137        mooring locations are shown in Fig. 1 and listed in Table 1. The AD-  
138        CPs are of make Teledyne RD Instruments, upward-looking, and operate at  
139        153.3 kHz. Though the Kanyakumari mooring had been deployed in 2009,  
140        the top ADCP had a frequency of 76.8 kHz till January 2016, over two  
141        years after the shift to 153.3 kHz off Kollam, Goa, and Mumbai (Chaudhuri  
142        et al., 2020). That’s why the Kanyakumari mooring was not included in  
143        the analysis of A22. We include it in our analysis because the 153.3 kHz  
144        measurements started in October 2017, when the additional three moorings  
145        were deployed in the EAS. The ADCP data used herein span the period  
146        October 2017 to December 2023, but there are data gaps at some locations  
(Table 1).

147        The moorings on the west-coast slope are serviced once a year during  
148        September–December depending on ship availability. Data was collected at  
149        hourly intervals with a 4 m bin size. The echoes at the surface render the  
150        data useless within roughly 10% of the transducer’s range ( $\sim$ 20 m) and this  
151        data is therefore discarded. We have followed the methodology laid down in  
152        A22 to derive the backscatter time series from ADCP echo intensity. Gaps  
153        up to two days are filled using the grafting method of Mukhopadhyay et al.  
154        (2017) and the graft-filled backscatter time series is converted to zooplankton  
155        biomass.

Off Kanyakumari, the top ADCP landed at a depth of  $\sim$ 300 m in the

<sup>158</sup> last deployment in January 2023 and backscatter data are not available in  
<sup>159</sup> the top ~120 m, precluding use of this record. Off Jaigarh, only a 76.8 kHz  
<sup>160</sup> ADCP could be deployed at the top; while this frequency does not matter  
<sup>161</sup> for the currents, it does matter for the backscatter, and the data from this  
<sup>162</sup> deployment is not used. Off Okha, data is not available for the entire upper  
~120 m for the second deployment (2018–2019).

<sup>164</sup> *2.2. The zooplankton biomass time series*

In situ biomass data from volumetric zooplankton samples are used to  
<sup>166</sup> convert the backscatter to biomass. The zooplankton samples were collected  
in the vicinity (~10 km) of the ADCP mooring site twice, once prior to  
<sup>168</sup> retrieval and again following the deployment of the mooring (Table 2). A  
multi-plankton net (MPN, 100  $\mu\text{m}$  mesh size, 0.5x0.5  $\text{m}^2$  mouth area) was  
<sup>170</sup> used to collect samples over pre-determined depth ranges; the water volume  
filtered was calculated by sampling depth range and mouth area. The timing  
<sup>172</sup> of sample collection was different throughout the MPN hauls owing to its  
dependence on the time of mooring retrieval, but from 2020 onward, the  
<sup>174</sup> depth range was standardized to fixed depth ranges of 0–25, 25–50, 50–75,  
75–100, and 100–150 m. Following numerous previous studies (A22; Flagg  
<sup>176</sup> and Smith, 1989; Heywood et al., 1991; Jiang et al., 2007), the backscatter  
was averaged in the vertical corresponding to the specific depth range of  
<sup>178</sup> the MPN haul for each site, and then linearly regressed with the biomass  
of corresponding depth range (Fig. 2). The zooplankton biomass in the  
<sup>180</sup> euphotic zone concentrates in the upper 10 m and this shift to near the  
surface is pronounced during the night. Yet, this should not be a concern  
<sup>182</sup> for the regression as it would simply show up as low backscatter at deeper  
depths during night-time corresponding to low biomass. It is important to

<sup>184</sup> note that the study is carried out using daily averaged biomass. Therefore,  
features associated with the DVM are eliminated (A22; Jiang et al., 2007).

<sup>186</sup> The zooplankton biomass time series (Fig. 3) is created from the above  
linear regression. ZSS is determined by taking the vertical integral of biomass  
<sup>188</sup> over the water column. Following A22, to ensure consistency in ZSS esti-  
mation across the time series, only those deployments with complete data  
<sup>190</sup> coverage throughout the full depth range of 24–120 m were included in the  
analysis. For a few years, the lack of data above  $\sim$ 140 m is due to the devia-  
<sup>192</sup> tion in the vertical position of the ADCP transducer in the water column. In  
spite of the care taken to position the instrument (mooring) at  $\sim$ 150–200 m  
<sup>194</sup> ( $\sim$ 1050–1100 m) depth, the process of mooring deployment, which is done  
from a steaming ship, implies that some deployments are shallower or deeper  
<sup>196</sup> owing to drift caused by floater-buoyancy and anchor-weight imbalance. It  
leads to a gap in the data at some mooring sites for some years. For exam-  
<sup>198</sup> ple, off Okha, data is not available for the entire upper 120 m depth for the  
second deployment (2018–2019). Data is also unavailable off Jaigarh from  
<sup>200</sup> the surface to  $\sim$ 60 m data during 2019–2022 and off Kollam below  $\sim$ 80 m  
during 2020–2021. There are also a few deployments during which no data  
<sup>202</sup> or bad data was recorded, e. g, off Udupi (2020–2021) and Kanyakumari  
(2022–2023); such bad data are discarded from standing-stock estimation.

<sup>204</sup> A decrease in biomass with increasing depth is observed at all seven  
locations (Fig. 3). To demarcate this expected decrease in biomass from the  
<sup>206</sup> more productive upper ocean to the less productive lower ocean, A22 used  
the  $215 \text{ mg m}^{-3}$  biomass contour (called  $z215$ ), and this contour is plotted  
<sup>208</sup> for both daily and monthly time series in Fig. 3; the depth of this contour  
is called  $D215$ . The lower biomass in the upper ocean off Kanyakumari and  
<sup>210</sup> Okha, however, led us to use the  $175 \text{ mg m}^{-3}$  for these locations. This

contour, whether  $D215$  or  $D175$ , cannot be plotted when data are missing,  
212 leading to some gaps in its time series.

The biomass decrease with depth, roughly defined as the difference be-  
214 tween mean biomass at 40 m and 104 m, is highest off Jaigarh and Mumbai,  
owing to the higher biomass in the upper ocean and lowest off Kanyakumari  
216 (Fig. 4, Table S2); this biomass decrease in the vertical is comparable at the  
other four locations. (A22 had reported that the decrease in biomass was  
218 lower off Kollam compared to Mumbai and Goa.)  $D215$ , like the biomass at  
40 m or 104 m, shows a seasonal variation: it moves up during the summer  
220 monsoon, when upwelling occurs, and down during the winter monsoon,  
when downwelling occurs. Note, however, that there is striking variation in  
222  $D215$  over the years sampled: indeed, the high difference between 40 m and  
104 m is due to a few years rather than being a standard feature of the entire  
224 record at a given location (Figs. 3,4). The mean and standard deviation of  
biomass are shown in Table S2. The sites with higher biomass tend to have  
226 higher variation over time, e. g., Mumbai, Jaigarh, and Kollam.

### 2.3. Other data sets

228 We also use data on temperature, salinity, MLD, oxygen, chl-*a* and  
satellite-derived sea-level anomalies (SLAs).

230 As in A22, in order to compare the changes in ZSS with the vertical  
movement of the thermocline, we use the monthly temperature climatology  
232 of Chatterjee et al. (2012) ( $1^\circ$  spatial resolution); the depth of the  $23^\circ\text{C}$   
isotherm (henceforth,  $D23$ ) is used as a proxy for the thermocline. Following  
234 A22, for comparison with the vertical movement of the oxycline, we use the  
monthly climatology of oxygen from the World Ocean Atlas 2013 (García  
236 et al., 2014). The oxygen concentration contour used as a proxy for the

oxycline is specific to each site owing to the presence of some locations  
238 within the OMZ and some locations outside its boundaries in the EAS.  
We use  $2.1 \text{ ml L}^{-1}$  for Kanyakumari and Kollam,  $3.2 \text{ ml L}^{-1}$  for Okha,  
240 and  $1.7 \text{ ml L}^{-1}$  for the other four locations; Kanyakumari, Kollam, and  
Okha lie outside the core of the OMZ in the EAS (see Fig. 1), but Okha  
242 is ventilated better owing to the intrusion of the Arabian Sea High Salinity  
Water (ASHSW; Rochford, 1964; Wyrtki et al., 1971) from farther north  
244 in the NEAS (Banse and Postel, 2009; Naqvi et al., 2006; Shankar et al.,  
246 2016). The MLD in the EAS is of the order of  $\sim 20\text{--}40 \text{ m}$  during the summer  
monsoon (Shetye et al., 1990; Shankar et al., 2005; Sreenivas et al., 2008),  
especially in the SEAS (Shenoi et al., 2005), but the MLD remains deep  
248 in the northern NEAS during winter (Shankar et al., 2016). As in A22,  
the climatological MLD is calculated using the temperature and salinity  
250 from the Chatterjee et al. (2012) data set using a density criterion: the  
MLD is defined as the depth at which the density increase from the surface  
252 corresponds to a  $0.5^\circ\text{C}$  decrease in temperature (Shenoi et al., 2004).

A22 used chl-*a* data from SeaWiFS, but this satellite ended service in  
254 2010; A22 could still use this data set because their use of chl-*a* was limited  
to a climatology. Since we want a time series of chl-*a*, we use the new  
256 chl-*a* product from Global Ocean Colour. Biogeochemical Level-4 data is  
obtained from E. U. Copernicus Marine Service Information. The daily  
258 data is available at a spatial resolution of 4 km, but, like all satellite chl-*a*  
data, has gaps due to clouds. Hence, to ensure a continuous time series,  
260 after applying the grafting method of Mukhopadhyay et al. (2017) on chl-*a*  
a trade-off is made between minimising the gaps in chl-*a* data and retention  
262 of at least 10 data points for computing the 30-day running-mean.

A22 used the depth of the  $20^\circ\text{C}$  isotherm, estimated from the climatology

<sup>264</sup> of Chatterjee et al. (2012), as a measure of the physical forcing (essentially upwelling or the vertical movement of the thermocline). Since this variable  
<sup>266</sup> is not available as a time series, we use the satellite-derived SLA as a proxy for the thermocline. The SLA data (daily L4 data on a  $0.25^\circ \times 0.25^\circ$   
<sup>268</sup> grid) was extracted for the period of interest (October 2017 to December 2023) from E. U. Copernicus Marine Service Information.

<sup>270</sup> **3. The seasonal cycle**

In this section, we discuss the seasonal climatology and the seasonal cycle  
<sup>272</sup> in the time series.

*3.1. Climatology of zooplankton biomass and standing stock*

<sup>274</sup> The monthly climatology of biomass, ZSS, and chl-*a* was computed from  
the monthly means, which were estimated for every month for which at least  
<sup>276</sup> 10 days of data were available. Therefore, since we have used all the available  
data at each location, the number of years for which the average is computed  
<sup>278</sup> is not the same at all locations because there are some gaps at some locations  
(Okha, for example). Yet, the similar behaviour of the A22 climatology  
<sup>280</sup> (2012–2020) and our climatology (2018–2022) off Kollam, Goa, and Mumbai  
(see Section S1) suggests that the basic features are strong aspects of the  
<sup>282</sup> seasonal climatology. Such strong features include the following (Fig. S1):  
the decrease in zooplankton biomass from the upper ocean to below *D*215 is  
<sup>284</sup> weaker off Kollam compared to Goa and Mumbai; there is high ZSS during  
the winter monsoon at all three locations in the EAS; there is a mismatch  
<sup>286</sup> in the chl-*a* peak, which occurs during the summer monsoon, and the ZSS  
peak, which occurs during the winter monsoon, off Kollam. While some  
<sup>288</sup> other details may vary between the two climatologies (higher zooplankton

biomass off Kollam and lower biomass off Goa in the new climatology), the  
290 basic features are consistent. We can infer that phytoplankton dominate  
in the SEAS and the microbial loop in the NEAS, a conclusion reached  
292 by both A22 and Shankar et al. (2019), which allowed the latter to infer  
explain why planktivorous (carnivorous) fish like the oil sardine (Bombay  
294 Duck) dominate in the SEAS (NEAS).

The four additional moorings throw more light on this transition from  
296 a phytoplankton-dominated ecosystem in the SEAS to a microbial-loop-  
dominated ecosystem in the NEAS. We find a decrease in the mean chl-*a*  
298 from Kollam ( $0.58 \text{ mg m}^{-3}$ ) to Jaigarh ( $0.28 \text{ mg m}^{-3}$ ), and an increase  
farther north in the NEAS (Fig. 5, Table S1). The change in the range  
300 or standard deviation (SD) of chl-*a* is, however, much more striking from  
Kollam to Okha: the range decreases from  $2.32 \text{ mg m}^{-3}$  off Kollam to just  
302  $0.24 \text{ mg m}^{-3}$  off Goa, before increasing again to  $0.7 \text{ mg m}^{-3}$  off Okha.  
Therefore, chl-*a* and the range of its variation are weaker in the CEAS  
304 and increase on either side of Jaigarh. The variation of ZSS is in striking  
contrast that of chl-*a*. The mean ZSS decreases from Kollam ( $24.6 \text{ g m}^{-2}$ )  
306 to Goa ( $21.2 \text{ mg m}^{-2}$ ), but increases to  $24.2 \text{ g m}^{-2}$  (practically the same  
as off Kollam) off Jaigarh before decreasing farther north. The range of  
308 ZSS variation, however, increases over twofold from  $4.1 \text{ g m}^{-2}$  off Kollam to  
 $9 \text{ g m}^{-2}$  off Jaigarh before decreasing again farther north. So the conclusion  
310 of a phytoplankton-dominated (microbial-loop-dominated) ecosystem in the  
SEAS (NEAS) inferred by A22 is strengthened by the new climatology:  
312 the transition tends to occur in the CEAS and can be considered to occur  
roughly north of Udupi owing to the significant decrease in the range of chl-*a*  
314 from Udupi to Goa.

The mooring location off Kanyakumari is distinct from the other six

316 mooring locations because the former lies at the junction of the Bay of Ben-  
gal and the Arabian Sea, in the regime of the seasonally reversing monsoon-  
318 current system (Shankar et al., 2002); the other six moorings lie on the  
slope off the Indian west coast. Therefore, we excluded Kanyakumari from  
320 the above discussion of chl-*a* and ZSS variation along the west-coast slope.  
This change in location *vis-a-vis* the west coast is seen in the chl-*a* and ZSS  
322 variation off Kanyakumari, where we find a high range of chl-*a* about a high  
mean chl-*a*, while the ZSS shows a low range of variation about a low mean  
324 (Fig. 5, Table S1). Off Jaigarh, in contrast, we find a high range of ZSS and  
a negligible range of chl-*a* about a low mean chl-*a*.

326 *3.2. Seasonal cycle and variability*

This seasonal cycle is evident in the time series (Fig. 4) and in the wavelet  
328 power spectra (see Section S2.1 for a brief discussion of wavelet analysis) of  
the biomass at 40 m and 140 m (Fig. 6) and the ZSS (Fig. 7). It is also  
330 seen in the biomass filtered in the seasonal band (see Section S2.2 for a brief  
discussion of filtering) of 100–400 days (Fig. 8) to extract only the seasonal  
332 variability, i. e., variability at a period of over three months so that it can  
be captured to an extent in a monthly time series. The wavelet spectra  
334 of biomass (Fig. 6) show high variability, denoted by the reddish colours,  
at all locations, but the strength of this variability is not the same. Off  
336 Kanyakumari, for example, the variability in the seasonal band is low, as  
indicated by the colour at both depths; in contrast, the seasonal variability  
338 appears strong in the wavelet spectra off Goa and Mumbai. In the filtered  
plot (Fig. 8), this change from Kanyakumari to Jaigarh is seen in the weaker  
340 shades of red and blue off Kanyakumari compared to the deeper shades off  
Jaigarh. The utility of the wavelet spectrum and the filtered biomass lies,

<sup>342</sup> however, in their ability to show how this seasonal variability, indicated by  
<sup>344</sup> the wavelet power or the colour shade, changes over time. For example, the  
<sup>346</sup> change in shades shows that the seasonal cycle is weak in both the wavelet  
spectrum of biomass at 40 m and the filtered biomass off Kollam during  
2020 and increases from 2021 onwards off Goa.

Note also that the colour often switches in the filtered plot from red  
<sup>348</sup> (positive deviation from the mean) to blue (negative deviation from the  
mean) around  $D175$  or  $D215$  (Fig. 8), which are defined using the monthly  
<sup>350</sup> time series of biomass, pointing to the role of this contour in separating  
the upper and lower ocean with respect to the zooplankton biomass. When  
<sup>352</sup> such a change of colour occurs, the positive and negative deviations on either  
side of the curve cancel each other in the vertical integral to determine ZSS,  
<sup>354</sup> this behaviour occurs over timescales ranging from intraseasonal to annual  
(Fig. S3). Hence, since such a change across  $D175$  is seen frequently off  
<sup>356</sup> Kanyakumari, the ZSS at this location shows a negligible variation, leading  
to a low SD in the climatology (Fig. 5, Table S1, Fig. S3) and over the time  
<sup>358</sup> series (Table S4). The SD increases in the CEAS, but decreases again in the  
NEAS (Table S4).

<sup>360</sup> Another feature noted by A22 and striking in the climatological ZSS  
(Fig. 5) is the asymmetry in time: the increase from the minimum dur-  
<sup>362</sup> ing the summer monsoon occurs much faster than the decrease from the  
maximum during the winter monsoon. This asymmetry, which is more pro-  
<sup>364</sup> nounced in the NEAS and CEAS (Fig. 5, Table S1), is a consequence of the  
temporal asymmetry in the monsoon winds and the resulting asymmetry  
<sup>366</sup> in the circulation (see, for example, Shankar et al., 2002, 2019): this vari-  
ability has been noted earlier in the west-coast alongshore currents (Amol  
<sup>368</sup> et al., 2014; Chaudhuri et al., 2020). As a result, there is significant variabil-

ity at the semi-annual period ( $\sim$ 180 days) in addition to the annual period (~365 days). Amol et al. (2014) split the seasonal variability of the current in the 100–400-day period band into two distinct bands, the annual band in the period range 300–400 days and the intra-annual band in the period range 100–250 days. The wavelet spectra show that the variability in the intra-annual band of  $\sim$ 100–250 days is not confined to the semi-annual period of 180 days, but extends to lower periods within this band. In the currents, variability around  $\sim$ 120 days has been noted (Amol et al., 2014; Chaudhuri et al., 2020), and variability around this period is also seen in the biomass (Fig. 6) at some locations. For example, off Kollam, the wavelet spectrum at 40 m shows variability around  $\sim$ 180 days in 2019–2020, but it is stronger at lower periods within this intra-annual band in 2021–2022. In general, the annual band for zooplankton biomass tends to be weaker than the intra-annual band (Figs. 6,S2, Table S3). Even within the weak seasonal cycle off Kanyakumari, variability is stronger in the intra-annual band compared to the annual band (Fig. S2, Table S3).

#### 4. Interannual variability

Interannual variability of the monthly time series may be considered to occur in two ways. First, there can be years in which the biomass or ZSS changes in one direction throughout the year, implying a significant deviation from the seasonal cycle, but at a period clearly different from variability within a season. Second, there can be a variability that is captured at a period higher than a year in a Fast Fourier Transform (FFT) or a wavelet spectrum.

The first kind of interannual variability is obvious from a comparison

394 of the biomass climatology (Fig. 5) and the biomass time series (Fig. 3).  
It is clear, for example, that the high climatological biomass above  $D_{215}$   
396 off Kollam during the summer monsoon is due to the high biomass occur-  
ring during a few years: the red colour, implying high wavelet power, is  
398 seen in 2022 and to a lesser extent in 2021 and 2022, but it is missing in  
earlier years. A more striking case occurs during 2020, when the biomass  
400 off Kollam collapsed over the entire depth range of sampling (Fig. 3; see  
Section S3) and this lower biomass is clearly seen in the biomass curves at  
402 40 m and 140 m (Fig. 4). A consequence of this collapse in zooplankton  
biomass is the significantly lower ZSS during 2020 off Kollam (Fig. 4). Such  
404 deviations, but usually of a weaker magnitude, from the expectation of the  
seasonal climatology occur fairly frequently at all locations. Off Goa, the  
406 climatology of A22 shows higher biomass above  $D_{215}$  than does the new cli-  
matology (Fig. S1); an examination of the data for 2012–2020 shows lower  
408 biomass during the summer monsoon in most of the years sampled in the  
new climatology compared to that of A22, leading to lower power around  
410 the annual band ( $\sim 360$  days) in the wavelet spectrum in the second half of  
the record (Fig. 9).

412 The second kind of interannual variability requires a change that occurs  
over more than a year. A22 noted the presence of this second kind of inter-  
414 annual variability off Kollam: the wavelet spectrum showed high power in a  
band around 720 days or roughly two years, but it was outside the wavelet  
416 cone of influence, implying that the time series was too short for the seeming  
quasi-biennial oscillation (QBO; Mooley and Parthasarathy, 1984; Bhalme  
418 et al., 1987), a well-known signal in Indian monsoon rainfall and therefore of  
monsoon variability, to be statistically significant. The persistent signal did,  
420 however, suggest a longer record would prove its existence off Kollam. An

examination of the wavelet spectrum over 2012–2022 shows a strong signal  
422 at this period during 2012–2018 (Fig. 9), but it weakens after that and the  
interannual band seems to shift to higher periods (Fig. 9). The QBO signal  
424 is also seen off Mumbai in the middle of the record, but appears at a higher  
period before 2017 and after 2021; it is weaker off Goa and appears outside  
426 the cone of influence (Fig. 9).

## 5. Intraseasonal variability

428 Apart from interannual variability, A22 also commented on the existence  
of intraseasonal variability in the daily biomass data obtained from  
430 the ADCP backscatter. Though they did not analyse it, A22 pointed out  
that this variability within a season is not small.

### 432 5.1. The wavelet spectrum

That this intraseasonal variability is strong is clearly seen in the deviation  
434 of the light-coloured curves for the daily data from the darker curves for  
the 30-day running mean of the biomass at 40 m and 104 m, and in the ZSS  
436 (Fig. 4). These significant deviations lead to a clear signal in the wavelet  
power at periods below 90 days for the 40 m and 104 m biomass (Fig. 6).  
438 Unlike the wavelet power at the seasonal time scales, which tends to be  
continuous in, say, the annual band for a year or more, the intraseasonal  
440 wavelet power is patchy, as has been seen earlier for the currents (Amol  
et al., 2014; Mukherjee et al., 2014; Chaudhuri et al., 2020; Mukhopadhyay  
442 et al., 2020). This patchiness is a consequence of the intraseasonal biomass  
bursts not occurring throughout the year or the time series, but on occasions  
444 within a season. The intraseasonal variability is prominent in the 30–90-day

band in the wavelet power spectrum, but there is also variability at periods shorter than 30 days (Fig. 6). For the currents, the lower bound used was  $\sim$ 5 days in order to filter out inertial currents off Kanyakumari, which has the highest inertial period of the seven locations (Amol et al., 2014; Chaudhuri et al., 2020). We retain this lower limit for our analysis of the intraseasonal variability of biomass and ZSS, i. e., we define the intraseasonal variability to occur in the period range of 5–90 days, with the 30–90-day (5–30-day) band constituting the “low-frequency” (“high-frequency”) parts of the intraseasonal spectrum; the low-frequency part of this band is marked by the horizontal lines in the wavelet plots.

The wavelet power is not normalised in this analysis. Therefore, even if the amplitude is the same at two different periods, the wavelet power will be less for the higher frequency (<https://paos.colorado.edu/research/wavelets/faq.html>). Hence, we cannot infer from the red (yellow) colours for the seasonal (intraseasonal) band in the wavelet spectrum (Fig. 6) that variability is higher in the seasonal band. Though this limitation of the wavelet spectrum can be overcome by normalising the wavelet power, we prefer to apply band-pass filters to extract the variability in the intraseasonal band (Fig. 10), as done earlier for the seasonal cycle (Fig. 8), because the result of this filtering is more intuitive.

### 5.2. Range of intraseasonal variability

Filtering the biomass with a band-pass filter (Fig. 10) suggests that the biomass range in the 5–90-day or intraseasonal band is comparable to that in the seasonal band (Fig. 8) and it often exceeds the seasonal range. (As noted earlier for the filtered plot of the seasonal cycle, the filtered intraseasonal biomass shows the deviation from the mean, leading to both positive

(red) and negative (blue) values.) The short time scale associated with the  
472 intraseasonal band makes it difficult to draw inferences from a plot of the entire time series (Fig. 10); hence, we present the analysis for 2019. This  
474 year is chosen because this deployment was not at the beginning or end of the time series (See Section S2 for the impact of filtering at the ends of  
476 the time series.) and there are fewer data gaps in the daily biomass time series. Note that our interest here is limited to showing that there is strong  
478 intraseasonal variability in zooplankton biomass, not in the details of this variability for any year (including 2019). Hence, we show only the Kollam  
480 figure for 2019 here (Fig. 11); the figures for the other locations are available in the supplement (Figs. S4–S9).

482 The expanded time axis shows that the range of biomass at 40 m in the 5–  
90-day band (Fig. 11b) is comparable to that in the seasonal band (Fig. 11a)  
484 off Kollam. There are, however, significant periods when intraseasonal vari-  
ability is weak (lighter shades of blue and red in Fig. 11b); these relatively  
486 quiescent periods are compensated by the occasions on which the intrasea-  
sonal range is significantly higher than the seasonal range (Fig. 11a,b,c). The  
488 daily biomass at 40 m is therefore determined by significant contributions  
from both seasonal and intraseasonal bands, with the relative contributions  
490 changing through the year: strong intraseasonal bursts lasting roughly a month are seen from the end of July through October (Fig. 11c). This re-  
492 sult, that the range of intraseasonal variability is comparable to the seasonal range, is also true for the rest of the time series off Kollam (Figs. 8,10), lead-  
494 ing to the SD for both bands being comparable at 40 m (Table S3). The same comparison holds off Udupi (Figs. 10,S5, Table S3), which lies just  
496 north of the boundary between the SEAS and the CEAS. Off Kanyakumari, however, the significantly weaker seasonal cycle (Fig. 8) leads to a

<sup>498</sup> higher range (Fig. S4) and SD (Table S3) for the intraseasonal band. The  
<sup>500</sup> higher range of the intraseasonal band is also evident off Goa (Fig. S6) and  
Jaigarh (Fig. S7) in the CEAS (Fig. 10, Table S3). A stronger seasonal cy-  
cle at NEAS compared to the CEAS implies that range of the seasonal and  
<sup>502</sup> intraseasonal bands is again comparable off Mumbai (Fig. S8, Table S3).  
Off Okha, the data gaps imply that the filled part of the seasonal band is  
<sup>504</sup> small (Fig. 8); hence, it is difficult to attach much significance to the higher  
intraseasonal range indicated by the high SD in this band (Table S3).

<sup>506</sup> At 104 m, i. e., below  $D215$  or  $D175$ , the range of the intraseasonal  
band is less than at 40 m off Kanyakumari (Fig. S4c), Kollam (Fig. 11c),  
<sup>508</sup> and Udupi (Fig. S5c), i. e., in the SEAS (Table S3). The range at both  
depths is comparable at the other locations. The intraseasonal range is  
<sup>510</sup> higher than the seasonal range off Kanyakumari and Jaigarh, lower than the  
seasonal range off Udupi, and of a similar magnitude at the other locations,  
<sup>512</sup> including Kollam (Figs. 8,10,11,S4–S9, Table S3). Therefore, even the non-  
monotonic pattern for the intraseasonal range that is suggested by the data  
<sup>514</sup> at 40 m is not applicable at 104 m.

### *5.3. Spikes in biomass*

<sup>516</sup> Striking at both 40 m and 104 m, however, is the seemingly higher range  
of the daily biomass than is indicated by an addition of the biomass in the  
<sup>518</sup> seasonal and intraseasonal bands (Figs. 11c,S4c–S9c). Part of this difference  
may be due to interannual variability, i. e., biomass varying at periods higher  
<sup>520</sup> than  $\sim 400$  days. Therefore, we applied a 5-day low-pass filter to the biomass  
to include this variability at time scales longer than the seasonal, and com-  
<sup>522</sup> pared the resulting curve with the daily biomass (Figs. 11d,S4d–S9d). The  
two curves almost overlap, suggesting that almost the entire variability of

524 the daily biomass curve at any depth can be explained by adding the vari-  
ability in the intraseasonal, seasonal, and interannual bands. The slight  
526 difference between the black and red curves (blue and cyan curves) for the  
low-passed and daily biomass at 40 m (104 m) suggests, however, that there  
528 is some variability at periods shorter than 5 days. An example of such a  
difference at 40 m occurs towards the end of July off Kollam (Fig. 11d).

530 Subtracting the 5-day low-passed biomass from the daily biomass shows  
the existence of spikes in the daily biomass (Figs. 11e,S4e–S9e). On several  
532 occasions, these spikes exceed one SD (dark grey background) and they  
exceed two SD (light grey background) on a few occasions. Examples of  
534 spikes exceeding two SD at 40 m are seen towards the end of July and  
August and in September off Kollam (Figs. 11e,S11). Similar spikes are  
536 seen in the biomass at 104 m, but fewer of these spikes exceed one SD or  
two SD: one spike exceeding two SD occurs in the last week of October off  
538 Kollam (Fig. S12). Such spikes, which extend the peaks in the daily biomass  
above the sum of the seasonal and intraseasonal bands, are also evident at  
540 the other six locations (Figs.S4e–S9e); the largest spikes occur off Jaigarh  
(Fig. S7e) at both 40 m (Fig. S11) and 104 m (Fig. S12).

542 These spikes, particularly in comparison to one SD, occur at random  
throughout the year. The positive spikes are caused by an increase in the  
544 biomass over a day or a few days, with lower biomass on either side of this  
increase. The negative spikes are caused by a decrease in biomass with  
546 respect to the higher biomass before and after this spike.

#### *5.4. Variation in standing stock*

548 The ZSS is obtained by integrating the biomass in the vertical, implying  
contributions from both above and below  $D215$  or  $D175$ . The mean biomass

550 is considerably less below this contour (Table S2), but the variability about  
this mean also matters. In the SEAS (Kanyakumari and Kollam), both  
552 seasonal and intraseasonal SD are much higher at 40 m (Table S3). Off  
Udupi, the seasonal range is comparable at these depths, but the intrasea-  
554 sonal range is high, as in the SEAS. The CEAS emerges as a regime where  
changes occur. Off Goa, the seasonal and intraseasonal ranges are compa-  
556 rable at these depths, but the behaviour is different off Jaigarh, where the  
intraseasonal ranges are comparable even though the seasonal range is much  
558 less at 40 m. In the NEAS, both seasonal and intraseasonal ranges are com-  
parable. (Note that the seasonal range off Okha is based on a short record.)  
560 There are occasions when high variability in the 30–90-day band is seen at  
both depths in the wavelet spectrum (Fig. 6) and in the filtered biomass  
562 (Fig. 10); an example is during August–November 2018 off Udupi, Goa, and  
Jaigarh in the CEAS. Variability in this band is also seen off Kollam and  
564 Mumbai during August–November 2018, but it is clearly weaker and more  
short-lived (Figs. 6,10).

566 In both bands, seasonal (Fig. 8) or intraseasonal (Figs. 10,11b,c,S4b,c–  
S9b,c), the deviation from the mean is not always in the same direction  
568 above and below  $D215$  or  $D175$ . Off Kollam, for example, the deviation of  
biomass at 40 m and 104 m is negative during February and August and  
570 positive during much of October in 2019; at other times, or over most of  
the year, the deviation has opposite signs (Fig. 11c). This tendency for the  
572 intraseasonal deviation to be of opposite sign at 40 m and 104 m is also seen  
often during the year at the other locations (Figs. S4c–S9c).

574 As expected, the variation of ZSS tends to be high when the variation  
of biomass above and below  $D215$  (or  $D175$ ) is in the same direction. An  
576 example is seen off Kollam in February 2019. The seasonal biomass devia-

tion at both 40 m and 104 m is negative (Fig. 11a,c), leading to a negative  
578 deviation throughout February in the seasonal ZSS (Fig. 11f). The intraseasonal deviation is also largely negative during February, save a short-lived  
580 positive burst in the beginning of the second half of the month (Fig. 11b,c).  
As a result, the intraseasonal ZSS deviation is largely negative, but with a  
582 short-lived positive burst (Fig. 11f). The strong negative seasonal bias implies,  
584 however, a negative deviation in the daily ZSS throughout February 2019 off Kollam (Fig. 11f). This possible cancellation of the deviation from  
586 the mean above and below  $D215$  (or  $D175$ ) leads to a weak variation in the  
588 intraseasonal SD of ZSS at the seven locations (Table S4); the SD is highest  
590 off Kollam and Jaigarh, but the ratio of the highest (Kollam) and lowest (Okha, Goa)  
intraseasonal SD is less than 1.4; in comparison, the ratio of the highest (Jaigarh) and lowest (Okha, Kanyakumari) seasonal SDs is over 2.7 (Table S4).

Since the ZSS is an integral quantity, it is not surprising that its SD,  
592 whether seasonal or intraseasonal, is much smaller at  $\sim 5\%$  of the mean  
(Figs. 11f,S4f–S9f, Table S4). For comparison, the SD of biomass varies  
594 from  $\sim 15\text{--}20\%$  (Figs. 11c,S4c–S9c, Table S3).

## 6. Discussion

### 6.1. Summary

Though A22's data set covered a different period (2012–2020) than our  
598 data set (2017–2023), the monthly climatologies off Kollam, Goa, and Mumbai estimated using them are similar; the differences are relatively minor (see  
600 Section S1, Fig. S1). The additional four moorings provide a clearer picture of the south–north transition on the continental slope in the EAS; biomass

602 is higher above  $D215$  or  $D175$ , which shallows during the summer monsoon  
603 in the SEAS and deepens during the winter monsoon in the NEAS, with the  
604 CEAS exhibiting a gradual transition between these two EAS regimes.

As noted by A22, the climatological ZSS is asymmetric in time, with  
606 the rise from the minimum during the summer monsoon occurring much  
607 faster than the gradual fall from the maximum during the winter monsoon  
608 (Fig. 5). This asymmetry, more pronounced in the NEAS and CEAS, leads  
610 to a strong intra-annual cycle, with peaks at around  $\sim 180$  days (the semi-  
611 annual cycle) and  $\sim 120$  days, in addition to the annual cycle (Figs. 6). The  
612 intra-annual band is stronger than the annual band within the seasonal cycle  
(Figs. 6,S2, Table S3).

The biomass also shows interannual variability off Kollam, Goa, and  
614 Mumbai, for which we have a record longer than a decade (2012–2023);  
615 these interannual variations affect the climatological averages. Year-to-year  
616 deviations from the monthly climatology are evident, with the most striking  
617 deviation occurring off Kollam in 2020, when the biomass was low over the  
618 entire deployment (see Section S3, Fig. S10). There is also variability at  
619 periods longer than the seasonal. The QBO reported off Kollam by A22  
620 is seen during 2012–2018; this QBO occurs sporadically off Mumbai and a  
621 weak signal is seen off Goa as well.

622 A key finding from the biomass data is the significant intraseasonal vari-  
623 ability (the 5–90-day band), which is at least comparable to the seasonal  
624 cycle (the 100–400-day band; Figs. 11,S4–S9, Table S3). The range of in-  
625 traseasonal variability is significantly higher off Kanyakumari owing to the  
626 low seasonal range, but the intraseasonal and seasonal ranges are compara-  
627 ble off Kollam and Udupi in the SEAS. The intraseasonal range is higher  
628 than the seasonal range off Goa and Jaigarh in the CEAS, but they are again

comparable in the NEAS (Table S3). This strong intraseasonal variability in  
630 biomass does not, however, lead to a comparably strong intraseasonal vari-  
ability in the ZSS because the ZSS is determined by the variation both above  
632 and below  $D215$  (or  $D175$ ) and the deviation from mean is often in opposite  
directions (Figs. 11,S4–S9). The intraseasonal variability also includes sharp  
634 spikes for a day or more, but less than five days (Figs. 11e,S4e–S9e). Several  
of these spikes, which occur intermittently throughout the year, exceed one  
636 SD and some exceed even two SD.

## 6.2. *The role of the physical forcing*

638 A22 showed that vertical movement of the climatological  $D215$  off Kol-  
lam, Goa, and Mumbai followed that of  $D23$ , the depth of the  $23^{\circ}\text{C}$  isotherm  
640 and therefore a measure of the vertical movement of the thermocline. This  
association also holds for our climatology of biomass (for  $D215$  or  $D175$ )  
642 at all seven locations (Fig. 5). Our biomass climatology represents a dif-  
ferent period than that of A22. Yet, this result still holds, implying that  
644 climatological upwelling and downwelling, which would move  $D23$  up and  
down, force a similar vertical movement of the climatological  $D215$  or  $D175$ ,  
646 the contour separating the high-biomass upper ocean from the low-biomass  
lower ocean. Hence, in a climatological sense, we find validation for A22’s  
648 result linking the physical forcing to the changes in biomass via the changes  
in oxygen as seen in the vertical movement of the oxycline (Fig. 5).

650 A proxy for  $D23$  is the sea level, which decreases (increases) or shows a  
negative (positive) anomaly during upwelling (downwelling), when  $D23$  rises  
652 (falls) or moves up (down). As expected (see, for example, Shankar, 2000),  
the climatological SLA mirrors the climatological  $D23$  (Fig. 5), suggesting  
654 the use of satellite-derived SLA as a proxy for  $D23$ , for which a time series is

not available on the continental slope of the EAS. A qualitative “eyeballing”  
656 of the data suggests that low (high) SLA, associated with upwelling (down-  
welling), co-occurs with high (low) biomass off Kollam in 2019 (Fig. 11d).  
658 To test this hypothesis, we carried out a wavelet coherence analysis to in-  
fer any possible link between the variation of SLA and biomass or ZSS at  
660 seasonal or intraseasonal time scales.

The analysis (figures not shown) did not show any conclusive relation.  
662 The coherence was weak and patchy even at the seasonal time scale. A  
possible reason for this lack of coherence is that the SLA, unlike biomass, is  
664 dominated by the annual cycle (the band picked by a 300–400 days band-  
pass filter) off Kollam, Goa, and Mumbai (Fig. 5). So it is not easy to  
666 quantify this expected relation between SLA and biomass at 40 m even at  
the seasonal time scale.

668 Not surprisingly, this lack of coherence extends to intraseasonal vari-  
ability (Figs. 5,11d,S4d–S9d). Even during August–November 2018, when a  
670 seemingly “coherent” biomass variation seems to occur off Udupi, Goa, and  
Jaigarh in the intraseasonal band (Figs. 6,10; see Section 5.4), the coherence  
672 between SLA and biomass tends to be extremely patchy at these locations  
(figures not shown), making it difficult to draw unambiguous conclusions  
674 about the link between the vertical movement of the thermocline and the  
upper-ocean (above  $D_{215}$  or  $D_{175}$ ) biomass.

676 The above analysis, though inconclusive, leads to one useful conclusion:  
qualitative associations between variables may not imply a cause-and-effect  
678 relationship even if based on a sound theoretical basis.

### *6.3. What sustains the zooplankton?*

680     Satellite-derived chlorophyll (chl-*a*) data are available as a daily time  
681     series, but with several gaps. Since these gaps preclude the creation of even  
682     a continuous, 10-day-low-pass time series, we use monthly chl-*a* data; daily  
683     data are plotted as curves where possible, but not subject to filtering or  
684     wavelet analysis. The lower temporal resolution implies that a significant  
685     part of the intraseasonal spectrum cannot be analysed.

686     Though one expects biomass and even ZSS to respond to chl-*a*, A22  
687     showed that the relation is not straightforward. The long time series avail-  
688     able off Kollam, Goa, and Mumbai shows that the biomass peaks do not  
689     necessarily follow the chl-*a* peaks (Fig. 9) even at the seasonal time scale  
690     resolved by the monthly time series. Neither is an increase in the magnitude  
691     of chl-*a* matched by an increase in that of the biomass at 40 m or of ZSS.  
692     Hence, wavelet coherence analysis (figures not shown) shows high wavelet  
693     coherence in the annual band, but the phase of chl-*a* does not lead that of  
694     biomass or ZSS, ruling out a quantitative cause-and-effect relationship. Yet,  
695     if we ignore this phase mismatch, there are instances when similar intrasea-  
696     sonal variation is seen in chl-*a* and biomass. Examples include high wavelet  
697     power at a period just above ~90 days off Kollam during the first half of  
698     2019 and through most of 2021–2022. The classical food web is also active  
699     and sometimes dominant in determining the surface ocean biomass as seen  
700     in Kanyakumari during July 2019 (Fig. S4e,f). It is difficult, however, to  
701     see this relation unequivocally in these curves.

702     The biomass data at 40 m also show spikes — implying variability at  
703     periods shorter than five days (see Section 5.3) — throughout the year,  
704     irrespective of whether there is a seasonal or intraseasonal peak in chl-*a*  
(Figs. 11e,S4e–S9e). Examples include spikes exceeding two SD in the 40 m

706 biomass off Kollam towards the end of August and during September 2019,  
when the chl-*a* has already declined from its July seasonal peak (Fig. 11e).  
708 Off Kanyakumari (Fig. S4c,d,), the biggest spike and the highest intrasea-  
sonal peak in the 40 m biomass occur during a short-lived increase in chl-*a*  
710 in September, but this chl-*a* peak is far weaker than the peak in July 2019,  
when the chl-*a* peak is over four times higher, but with smaller spikes and  
712 a weaker intraseasonal peak in the biomass at 40 m. A similar behaviour  
is seen at the other five locations (Figs. S5–S9): off Mumbai (Fig. S8), for  
714 example, the big spike in June 2019 precedes the increase in chl-*a* by several  
days.

716 One drawback of satellite chl-*a* data is that the satellite cannot see be-  
yond  $\sim$ 30 m from the surface (maximum is  $\sim$ 40 m in clear water; André,  
718 1992), implying that not all of the phytoplankton biomass is part of the  
satellite estimate. Though the chl-*a* data set used here includes the pi-  
720 cophytoplankton, it cannot capture the picophytoplankton that dominate  
below  $\sim$ 40 m along with the microbial loop. Picoplankton (Campbell and  
722 Carpenter, 1986; Campbell et al., 1998; Bemal et al., 2018) and the micro-  
bial loop (Azam et al., 1983; Madhupratap et al., 1996a,b; Anil et al., 2021)  
724 have been shown to be important components of the marine food web in the  
Arabian Sea.

726 What the zooplankton biomass time series at these seven locations show  
is that the picophytoplankton and microbial loop must be dominating over  
728 the classical food web (Bemal et al., 2018; Anil et al., 2021) over a significant  
part of the year throughout the EAS. It is this non-classical part of the food  
730 web that probably sustains the significant intraseasonal bursts seen in the  
biomass data.

732 *6.4. Caveats and strengths*

A22 discussed the caveats and strengths of using ADCP backscatter to  
734 map the variability of zooplankton biomass and standing stock.

They noted the lack of data in the near-surface regime, a consequence of  
736 the echoes from the air-sea interface. Since  $\sim 10\%$  of the range of the ADCP  
is lost, data are lost over the top  $\sim 20$  m for a 153.3 kHz ADCP moored at  
738  $\sim 150$  m. Another limitation is that the cruises used for *in situ* sampling are  
restricted to one season, September–December, owing to the constraints im-  
740 posed by weather conditions on mooring operations and availability of ship  
time. This limitation is partly obviated by the large range in backscatter  
742 and biomass over the sampled depth range from  $\sim 24$ –140 m: the significant  
decrease in backscatter below  $D_{215}$  (or  $D_{175}$ ) leads to a range that is un-  
744 likely to be exceeded by sampling in other seasons. Yet, that zooplankton  
abundance and biomass are not necessarily related (see, for example, Mad-  
746 hupratap et al., 1990; Ambriz-Arreola et al., 2018) implies that the seasonal  
change in species can have an impact on the distribution of points in the  
748 scatter plot (Fig. 2). Analysis using ship-based sampling in the EAS (Jad-  
hav and Smitha, 2024) shows a seasonal biomass difference of  $\sim 15 \text{ mg m}^{-3}$ ,  
750 comparable to our SD estimate of  $14 \text{ mg m}^{-3}$  (Fig. 2). Therefore, it is  
unlikely that sampling in other seasons will lead to a major change in the  
752 backscatter-biomass regression, but it would be good to exploit any oppor-  
tunity to broaden the sampling range. The absence of species information  
754 is, however, the most significant lacuna of the use of ADCP backscatter.  
Studies in the EAS show that even picoplankton are sufficiently differenti-  
756 ated that *Prochlorococcus* species attuned to low light do not bloom when  
exposed to high-nutrient conditions in the near-surface regime because of the  
758 light shock (Bemal et al., 2018). Even microbial communities show similar

sensitivity to environmental conditions (Khandeparker et al., 2025).

This biodiversity information is, nevertheless, lost even in satellite chl-*a* data, which are used to estimate the energy flux through the marine ecosystem. Zooplankton biomass estimated from acoustic backscatter provides the closest analogue to satellite chl-*a*. Thus, the chief merit of this method is obvious: traditional sampling cannot yield a time series of the kind presented above, precluding any analysis of the variability over the range of time scales seen in the backscatter data. For example, it is only with such a time series that it is possible to analyse the impact of climate modes like ENSO (El Niño Southern Oscillation; see, for example, Sikka, 1980) or the Indian-Ocean Dipole (IOD; Saji et al., 1999) on the interannual variation in zooplankton biomass and standing stock. In other words, the raw estimate of biomass is as biologically relevant — owing to its potential for estimating energy flux — as is the biodiversity that can be catalogued using MPN samples.

The time series of biomass, with its intraseasonal bursts and spikes, also calls into question the contours of biomass or ZSS drawn using cruise data. In the EAS, for example, it takes roughly a month to cover the Indian Exclusive Economic Zone (EEZ) from Kanyakumari to Okha (see, for example, Shetye et al., 1990, 1991; Vijith et al., 2022; Madhupratap et al., 1996a; Jyothibabu et al., 2010). It is certain, therefore, that this sampling cannot account for the spikes or the variability in at least the 5–30-day part of the intraseasonal band. This variability, evident at all mooring locations, implies that the error bar in these biomass or ZSS snapshots is likely too high to permit contouring of these variables using cruise data.

784    6.5. *Epilogue*

What we actually need is a synergy between the two methods because the  
786    two sets of information are not only complementary, but also relevant. This  
complementarity and relevance may be illustrated by the ADCP deployment  
788    off Kollam during October 2019 to December 2020. The backscatter —  
and therefore biomass — was low off Kollam throughout this deployment.  
790    Doubts regarding the instrument were generally laid to rest with a series of  
checks (see Section S3), but the clincher was the low biomass sampled using  
792    the MPN after deploying the ADCP in 2019 and before retrieving it in 2020  
(Table 2, Fig. 2). Indeed, it the time series that shows unambiguously that  
794    the biomass off Kollam was low throughout this 12–14-month period.

All methods — ship, satellite, or acoustics —, however, miss some in-  
796    formation. The obvious implication is that large parts of the marine food  
web, and therefore the energy flux through the marine ecosystem, is not  
798    measured. Some components, like picophytoplankton that are not captured  
in satellite chl-*a* and the microbial loop, are essentially unmeasurable. In  
800    this context, acoustic backscatter enables some constraints on the second  
trophic level, and our results from the EAS show that the picoplankton and  
802    microbial loop are critical for sustaining the observed zooplankton biomass  
and its variability. It is necessary for models to build the impact of even  
804    these difficult-to-measure or unmeasurable elements into their depiction of  
the marine food web in order to avoid the trap of the *McNamara fallacy*  
806    (Yankelovich, 1971).

## **Declaration of competing interest**

808        The authors declare that they have no known competing financial in-  
terests or personal relationships that could have appeared to influence the  
810 work reported in this article.

## **Acknowledgments**

812        This work was supported by ship time funded by CSIR (Council of Scien-  
tific and Industrial Research, New Delhi, India) and research funding from  
814 INCOIS (Indian National Centre for Ocean Information Services, Hyder-  
abad, India) under the COSINE (Current Observations and Simulations in  
816 the Indian EEZ) project, which is a part of the OSMART programme of  
the Ministry of Earth Sciences. The ADCP moorings are maintained by our  
818 colleagues from the mooring group; they are assisted by the CSIR-NIO ship  
cell during cruises and the data are archived by Ashok Kankonkar. Rahul  
820 Khedekar assisted in processing the backscatter data and Roshan D'Souza  
in analysing the zooplankton samples. D. Shankar acknowledges the insights  
822 gained from conversations with Lidita Khandeparker on bacteria and the mi-  
crobial loop and with A.C. Anil on marine ecosystems. Ranjan Kumar Sahu  
824 was supported by a fellowship from CSIR. This is CSIR-NIO contribution  
xxxx.

## **826 References**

Almén, A.K., Tamelander, T., 2020. Temperature-related timing of the  
828 spring bloom and match between phytoplankton and zooplankton. Mar.  
Biol. Res. 16, 674–682. 10.1080/17451000.2020.1846201.

- 830 Ambriz-Arreola, I., Gómez-Gutiérrez, J., Franco-Gordo, M., Plascencia-  
Palomera, V., Gasca, R., Kozak, E.R., Lavaniegos, B.E., 2018. Seasonal  
832 succession of tropical community structure, abundance, and biomass of  
five zooplankton taxa in the central Mexican Pacific. *Cont. Shelf Res.*  
834 168, 54–67. [10.1016/j.csr.2018.08.007](https://doi.org/10.1016/j.csr.2018.08.007).
- 836 Amol, P., Bemal, S., Shankar, D., Jain, V., Thushara, V., Vijith, V., Vinay-  
achandran, P.N., 2020. Modulation of chlorophyll concentration by down-  
welling Rossby waves during the winter monsoon in the southeastern  
838 Arabian Sea. *Prog. Oceanogr.* 186, 102365. [10.1016/j.pocean.2020.102365](https://doi.org/10.1016/j.pocean.2020.102365).
- 840 Amol, P., Shankar, D., Fernando, V., Mukherjee, A., Aparna, S.G., Fer-  
nandes, R., Michael, G.S., Khalap, S.T., Satelkar, N.P., Agarvadekar,  
842 Y., Gaonkar, M.G., Tari, A.P., Kankonkar, A., Vernekar, S., 2014. Ob-  
served intraseasonal and seasonal variability of the West India Coastal  
844 Current on the continental slope. *J. Earth Syst. Sci.* 123, 1045–1074.  
[10.1007/s12040-014-0449-5](https://doi.org/10.1007/s12040-014-0449-5).
- 846 André, J.M., 1992. Ocean color remote-sensing and the subsurface vertical  
structure of phytoplankton pigments. *Deep-Sea Res. Part A Oceanogr.*  
848 *Res. Pap.* 39, 763–779. [10.1016/0198-0149\(92\)90119-E](https://doi.org/10.1016/0198-0149(92)90119-E).
- Anil, A.C., Desai, D.V., Khandeparker, L., Krishnamurthy, V., Mapari, K.,  
850 Mitbavkar, S., Patil, J.S., Sarma, V.V.S.S., Sawant, S.S., 2021. Short term  
response of plankton community to nutrient enrichment in central eastern  
852 Arabian Sea: Elucidation through mesocosm experiments. *J. Environ.*  
*Manage.* 288, 112390. [10.1016/j.jenvman.2021.112390](https://doi.org/10.1016/j.jenvman.2021.112390).
- 854 Aparna, S.G., Desai, D.V., Shankar, D., Anil, A.C., Dora, S., Khedekar,

- R.R., 2022. Seasonal cycle of zooplankton standing stock inferred from  
856 ADCP backscatter measurements in the eastern Arabian Sea. *Prog.*  
*Oceanogr.* 203, 102766. [10.1016/j.pocean.2022.102766](https://doi.org/10.1016/j.pocean.2022.102766).
- Azam, F., Fenchel, T., Field, J.G., Gray, J.S., Meyer-Reil, L.A., Thingstad,  
858 F., 1983. The ecological role of water-column microbes in the sea. *Estuaries* 10, 257–263. [10.3384/meps010257](https://doi.org/10.3384/meps010257).
- Banse, K., 1968. Hydrography of the Arabian Sea shelf of India and Pak-  
862 istan and effects on demersal fishes, in: Deep-Sea Res. *Oceanogr. Abstr.*,  
Elsevier. pp. 45–79. [10.1016/0011-7471\(68\)90028-4](https://doi.org/10.1016/0011-7471(68)90028-4).
- Banse, K., 1995. Zooplankton: pivotal role in the control of ocean pro-  
864 duction: I. Biomass and production. *ICES J. Mar. Sci.* 52, 265–277.  
10.1016/1054-3139(95)80043-3.
- Banse, K., English, D.C., 2000. Geographical differences in seasonality of  
868 CZCS-derived phytoplankton pigment in the Arabian Sea for 1978–1986.  
*Deep-Sea Res. Part II Top. Stud. Oceanogr.* 47, 1623–1677. [10.1016/S0967-0645\(99\)00157-5](https://doi.org/10.1016/S0967-0645(99)00157-5).
- Banse, K., Postel, J.R., 2009. Wintertime convection and ventilation of the  
872 upper pycnocline in the northernmost Arabian Sea. *Geophysical Mono-*  
*graph Series* 185, 87–117. [10.1029/2008GM000704](https://doi.org/10.1029/2008GM000704).
- Barber, R.T., Marra, J., Bidigare, R.C., Codispoti, L.A., Halpern, D., John-  
874 son, Z., Latasa, M., Goericke, R., Smith, S.L., 2001. Primary productivity  
876 and its regulation in the Arabian Sea during 1995. *Deep-Sea Res. Part 2*  
*Top. Stud. Oceanogr.* 48, 1127–1172. [10.1016/S0967-0645\(00\)00134-X](https://doi.org/10.1016/S0967-0645(00)00134-X).

- 878 Batchelder, H.P., VanKeuren, J.R., Vaillancourt, R.D., Swift, E., 1995.  
880      Spatial and temporal distributions of acoustically estimated zooplankton  
882      biomass near the marine light-mixed layers station ( $59^{\circ}30'N$ ,  $21^{\circ}00'W$ ) in  
the north Atlantic in May 1991. *J. Geophys. Res. Oceans* 100, 6549–6563.  
882      [10.1029/94jc00981](https://doi.org/10.1029/94jc00981).
- 884 Bemal, S., Anil, A.C., Shankar, D., Remya, R., Roy, R., 2018. Picophy-  
886      toplankton variability: Influence of winter convective mixing and ad-  
vection in the northeastern Arabian Sea. *J. Mar. Syst.* 180, 37–48.  
886      [10.1029/2001GL013422](https://doi.org/10.1029/2001GL013422).
- 888 Bhalme, H.N., Rahalkar, S.S., Sikder, A.B., 1987. Tropical quasi-biennial  
890      oscillation of the 10-mb wind and Indian monsoon rainfall — implications  
for forecasting. *J. Climatol.* 7, 345–353. [10.1002/joc.3370070403](https://doi.org/10.1002/joc.3370070403).
- 892 Brock, J.C., McClain, C.R., 1992. Interannual variability in phytoplankton  
blooms observed in the northwestern Arabian Sea during the southwest  
monsoon. *J. Geophys. Res. Oceans* 97, 733–750. [10.1029/91JC02225](https://doi.org/10.1029/91JC02225).
- 894 Brock, J.C., McClain, C.R., Luther, M.E., Hay, W.W., 1991. The phy-  
toplankton bloom in the northwestern Arabian Sea during the south-  
west monsoon of 1979. *J. Geophys. Res. Oceans* 96, 20623–20642.  
896      [10.1029/91JC01711](https://doi.org/10.1029/91JC01711).
- 898 Campbell, L., Carpenter, E.J., 1986. Estimating the grazing pressure of  
heterotrophic nanoplankton on *Synechococcus* spp. using the sea water  
dilution and selective inhibitor techniques. *Mar. Ecol. Prog. Ser.* 33, 121–  
900      129.
- Campbell, L., Landry, M.R., Constantinou, J., Nolla, H.A., Brown, S.L.,

- 902 Liu, H., Caron, D.A., 1998. Response of microbial community structure  
to environmental forcing in the Arabian Sea. Deep-Sea Res. II Top. Stud.  
904 Oceanogr. 45, 2301–2325.
- 906 Chatterjee, A., Shankar, D., Shenoi, S.S.C., Reddy, G.V., Michael, G.S.,  
Ravichandran, M., Gopalkrishna, V.V., RamaRao, E.P., UdayaBhaskar,  
T.V.S., Sanjeevan, V.N., 2012. A new atlas of temperature and salinity  
908 for the North Indian Ocean. J. Earth Syst. Sci. 121, 559–593. [10.1007/s12040-012-0191-9](https://doi.org/10.1007/s12040-012-0191-9).
- 910 Chaudhuri, A., Shankar, D., Aparna, S.G., Amol, P., Fernando, V.,  
Kankonkar, A., Michael, G.S., Satelkar, N.P., Khalap, S.T., Tari, A.P.,  
912 Gaonkar, M.G., Ghatkar, S., Khedekar, R.R., 2020. Observed variability  
of the West India Coastal Current on the continental slope from 2009–  
914 2018. J. Earth Syst. Sci. 129, 57. [10.1007/s12040-019-1322-3](https://doi.org/10.1007/s12040-019-1322-3).
- 916 Cisewski, B., Strass, V.H., Rhein, M., Krägesky, S., 2010. Seasonal variation  
of diel vertical migration of zooplankton from ADCP backscatter time  
series data in the Lazarev Sea, Antarctica. Deep-Sea Res. Part I Oceanogr.  
918 Res. Pap. 57, 78–94. [10.1016/j.dsr.2009.10.005](https://doi.org/10.1016/j.dsr.2009.10.005).
- 920 Davis, R.E., Talley, L.D., Roemmich, D., Owens, W.B., Rudnick, D.L.,  
Toole, J., Weller, R., McPhaden, M.J., Barth, J.A., 2019. 100 years of  
922 progress in ocean observing systems. Meteorol. Monogr. 59, 3–1. [10.1175/AMSMONOGRAPHSD-18-0014.1](https://doi.org/10.1175/AMSMONOGRAPHSD-18-0014.1).
- 924 Deines, K.L., 1999. Backscatter estimation using broadband acoustic  
Doppler current profilers, in: Proceedings of the IEEE Sixth Working  
Conference on Current Measurement (Cat. No. 99CH36331), IEEE. pp.  
926 249–253. [10.1109/CCM.1999.755249](https://doi.org/10.1109/CCM.1999.755249).

- DeSousa, S.N., Dileepkumar, M., Sardessai, S., Sarma, V.V.S.S., Shirodkar,  
928 P.V., 1996. Seasonal variability in oxygen and nutrients in the central and  
eastern Arabian Sea. *Curr. Sci.* 71. [drs.nio.org/drs/handle/2264/35](http://drs.nio.org/drs/handle/2264/35).
- 930 Edvardsen, A., Slagstad, D., Tande, K.S., Jaccard, P., 2003. Assessing  
zooplankton advection in the Barents Sea using underway measurements  
932 and modelling. *Fish. Oceanogr.* 12, 61–74. [10.1046/j.1365-2419.2003.00219.x](https://doi.org/10.1046/j.1365-2419.2003.00219.x).
- 934 Flagg, C.N., Smith, S.L., 1989. On the use of the acoustic Doppler current  
profiler to measure zooplankton abundance. *Deep-Sea Res. Part A.*  
936 *Oceanogr. Res. Pap.* 36, 455–474. [10.1016/0198-0149\(89\)90047-2](https://doi.org/10.1016/0198-0149(89)90047-2).
- 938 García, H.E., Locarnini, R.A., Boyer, T.P., Antonov, J.I., Mishonov, A.V.,  
Baranova, O.K., Zweng, M.M., Reagan, J.R., Johnson, D.R., 2014. Dissolved  
oxygen, apparent oxygen utilization, and oxygen saturation. NOAA  
940 Atlas NESDIS 75 3. [data.nodc.noaa.gov/woa/WOA18/DOC/woa18\\_vol3.pdf](http://data.nodc.noaa.gov/woa/WOA18/DOC/woa18_vol3.pdf).
- 942 Greene, C.H., Wiebe, P.H., Pelkie, C., Benfield, M.C., Popp, J.M.,  
1998. Three-dimensional acoustic visualization of zooplankton patchiness.  
944 *Deep-Sea Res. Part II Top. Stud. Oceanogr.* 45, 1201–1217.  
[10.1016/S0967-0645\(98\)00034-4](https://doi.org/10.1016/S0967-0645(98)00034-4).
- 946 Greenlaw, C.F., 1979. Acoustical estimation of zooplankton populations 1.  
*Limnol. Oceanogr.* 24, 226–242. [10.4319/lo.1979.24.2.00226](https://doi.org/10.4319/lo.1979.24.2.00226).
- 948 Guerra, D., Schroeder, K., Borghini, M., Camatti, E., Pansera, M.,  
Schroeder, A., Sparnocchia, S., Chiggiato, J., 2019. Zooplankton diel  
950 vertical migration in the Corsica channel (north-western Mediterranean

- Sea) detected by a moored acoustic Doppler current profiler. *Ocean Sci.*  
952      15, 631–649. [10.5194/os-15-631-2019](https://doi.org/10.5194/os-15-631-2019).
- Hamilton, J.M., Collins, K., Prinsenberg, S.J., 2013. Links between ocean  
954 properties, ice cover, and plankton dynamics on interannual time scales  
in the Canadian Arctic Archipelago. *J. Geophys. Res. Oceans* 118, 5625–  
956 5639. [10.1002/jgrc.20382](https://doi.org/10.1002/jgrc.20382).
- Hays, G.C., 2003. A review of the adaptive significance and ecosystem  
958 consequences of zooplankton diel vertical migrations, in: *Migrations and*  
*Dispersal of Marine Organisms: Proceedings of the 37th European Ma-*  
960 *rine Biology Symposium held in Reykjavík, Iceland, 5–9 August 2002,*  
Springer. pp. 163–170. [10.1007/978-94-017-2276-6\\_18](https://doi.org/10.1007/978-94-017-2276-6_18).
- 962 Heywood, K.J., Howe, S.S., Barton, E.D., 1991. Estimation of zooplankton  
abundance from shipborne ADCP backscatter. *Deep-Sea Res. Part A.*  
964 *Oceanogr. Res. Pap.* 38, 677–691. [10.1016/0198-0149\(91\)90006-2](https://doi.org/10.1016/0198-0149(91)90006-2).
- 966 Hobbs, L., Banas, N.S., Cohen, J.H., Cottier, F.R., Berge, J., Varpe, Ø.,  
2021. A marine zooplankton community vertically structured by light  
across diel to interannual timescales. *Biol. Lett.* 17, 20200810. [10.1098/rsbl.2020.0810](https://doi.org/10.1098/rsbl.2020.0810).
- 970 Hood, R.R., Beckley, L.E., Wiggert, J.D., 2017. Biogeochemical and ecolog-  
ical impacts of boundary currents in the Indian Ocean. *Prog. Oceanogr.*  
156, 290–325. [10.1016/j.pocean.2017.04.011](https://doi.org/10.1016/j.pocean.2017.04.011).
- 972 Inoue, R., Kitamura, M., Fujiki, T., 2016. Diel vertical migration of  
zooplankton at the S1 biogeochemical mooring revealed from acous-

- 974       tic backscattering strength. *J. Geophys. Res. Oceans* 121, 1031–1050.  
10.1002/2015JC011352.
- 976       Jadhav, S.J., Smitha, B., 2024. Abundance distribution pattern of zooplankton associated with the eastern Arabian Sea monsoon system as  
978       detected by underwater acoustics and net sampling. *Acoust. Aust.* , 1–  
2210.1007/s40857-024-00336-w.
- 980       Jiang, S., Dickey, T.D., Steinberg, D.K., Madin, L.P., 2007. Temporal variability of zooplankton biomass from ADCP backscatter time series data  
982       at the Bermuda Testbed Mooring site. *Deep-Sea Res. Part I Oceanogr. Res. Pap.* 54, 608–636. 10.1016/j.dsr.2006.12.011.
- 984       Jyothibabu, R., Madhu, N.V., Habeebrehman, H., Jayalakshmy, K.V., Nair,  
986       K.K.C., Achuthankutty, C.T., 2010. Re-evaluation of ‘paradox of mesozooplankton’ in the eastern Arabian Sea based on ship and satellite observations. *J. Mar. Syst.* 81, 235–251. 10.1016/j.jmarsys.2009.12.019.
- 988       Kang, M., Oh, S., Oh, W., Kang, D.J., Nam, S., Lee, K., 2024. Acoustic  
990       characterization of fish and macroplankton communities in the Seychelles-Chagos Thermocline Ridge of the southwest Indian Ocean. *Deep-Sea Res. Part II Top. Stud. Oceanogr.* 213, 105356. 10.1016/j.dsr2.2023.  
992       105356.
- 994       Keerthi, M.G., Lengaigne, M., Lévy, M., Vialard, J., Parvathi, V.,  
996       de Boyer Montégut, C., Ethé, C., Aumont, O., Suresh, I., Akhil, V.P.,  
Muraleedharan, P.M., 2017. Physical control of interannual variations of  
the winter chlorophyll bloom in the northern Arabian Sea. *Biogeosci.* 14,  
3615–3632. 10.5194/bg-14-3615-2017.

- 998 Khandagale, P.A., Mhatre, V.D., Thomas, S., 2022. Seasonal and spatial  
 variability of zooplankton diversity in north eastern Arabian Sea along  
 1000 the Maharashtra coast. *J. Mar. Biol. Assoc. India* 64, 25–32. [mbai.org.in/php/journaldload.php?id=2618&bkid=128](http://mbai.org.in/php/journaldload.php?id=2618&bkid=128).
- 1002 Khandeparker, L., Kale, D., Hede, N., Anil, A.C., 2025. Application of functional metagenomics in the evaluation of microbial community dynamics  
 1004 in the Arabian sea: Implications of environmental settings. *J. Environ. Manag.* 373, 123449. [10.1016/j.jenvman.2024.123449](https://doi.org/10.1016/j.jenvman.2024.123449).
- 1006 Kumar, S.P., Narvekar, J., 2005. Seasonal variability of the mixed layer  
 in the central Arabian Sea and its implication on nutrients and primary  
 1008 productivity. *Deep-Sea Res. Part II Top. Stud. Oceanogr.* 52, 1848–1861.  
[10.1016/j.dsr2.2005.06.002](https://doi.org/10.1016/j.dsr2.2005.06.002). biogeochemical Processes in the North-  
 1010 ern Indian Ocean.
- 1012 Lévy, M., Shankar, D., André, J.M., Shenoi, S.S.C., Durand, F.,  
 de Boyer Montégut, C., 2007. Basin-wide seasonal evolution of the  
 Indian Ocean's phytoplankton blooms. *J. Geophys. Res. Oceans* 112.  
 1014 [10.1029/2007JC004090](https://doi.org/10.1029/2007JC004090).
- 1016 Li, M., Gargett, A., Denman, K., 2000. What determines seasonal and  
 interannual variability of phytoplankton and zooplankton in strongly es-  
 tuarine systems? *Estuar. Coast. Shelf Sci.* 50, 467–488. [10.1006/ecss.2000.0593](https://doi.org/10.1006/ecss.2000.0593).
- 1020 Liu, Y., Guo, J., Xue, Y., Sangmanee, C., Wang, H., Zhao, C., Khoki-  
 attiwong, S., Yu, W., 2022. Seasonal variation in diel vertical migra-  
 tion of zooplankton and micronekton in the Andaman Sea observed by a

- 1022 moored ADCP. Deep-Sea Res. Part I Oceanogr. Res. Pap. 179, 103663.  
10.1016/j.dsr.2021.103663.
- 1024 Madhupratap, M., Gopalakrishnan, T.C., Haridas, P., Nair, K.K.C., Ar-  
avindakshan, P.N., Padmavati, G., Paul, S., 1996a. Lack of seasonal  
1026 and geographic variation in mesozooplankton biomass in the Arabian  
Sea and its structure in the mixed layer. Curr. Sci. 71, 863–868.  
1028 [drs.nio.org/drs/handle/2264/2154](http://drs.nio.org/drs/handle/2264/2154).
- 1030 Madhupratap, M., Haridas, P., Ramaiah, N., Achuthankutty, C.T., 1992.  
Zooplankton of the southwest coast of India: abundance, composition,  
temporal and spatial variability in 1987. Oceanogr. Indian Ocean .
- 1032 Madhupratap, M., Kumar, S.P., Bhattathiri, P.M.A., Kumar, M.D.,  
Raghukumar, S., Nair, K.K.C., Ramaiah, N., 1996b. Mechanism of the  
1034 biological response to winter cooling in the northeastern Arabian Sea.  
Nature 384, 549–552. 10.1038/384549a0.
- 1036 Madhupratap, M., Nair, S.R.S., Haridas, P., Padmavati, G., 1990. Response  
of zooplankton to physical changes in the environment: coastal upwelling  
1038 along the central west coast of India. J. Coast. Res. , 413–426<http://www.jstor.org/stable/4297692>.
- 1040 Maraun, D., Kurths, J., 2004. Cross wavelet analysis: significance test-  
ing and pitfalls. Nonlin. Processes Geophys. 11, 505–514. 10.5194/  
1042 npg-11-505-2004.
- 1044 McCreary, J.P., Kohler, K.E., Hood, R.R., Olson, D.B., 1996. A four-  
component ecosystem model of biological activity in the Arabian Sea.  
Prog. Oceanogr. 37, 193–240. 10.1016/S0079-6611(96)00005-5.

- 1046 McCreary, J.P., Kundu, P.K., Molinari, R.L., 1993. A numerical investigation  
of dynamics, thermodynamics and mixed-layer processes in the Indian  
1048 Ocean. *Prog. Oceanogr.* 31, 181–244. [10.1016/0079-6611\(93\)90002-U](https://doi.org/10.1016/0079-6611(93)90002-U).
- 1050 McCreary, J.P., Murtugudde, R., Vialard, J., Vinayachandran, P.N., Wiggert,  
J.D., Hood, R.R., Shankar, D., Shetye, S.R., 2009. Biophysical processes in the Indian Ocean. *Indian Ocean Biogeochem. Processes Ecol.*  
1052 *Variab.* 185, 9–32. [10.1029/2008GM000768](https://doi.org/10.1029/2008GM000768).
- 1054 Mooley, D.A., Parthasarathy, B., 1984. Fluctuations in all-India summer  
monsoon rainfall during 1871–1978. *Clim. Change* 6, 287–301. [10.1007/BF00142477](https://doi.org/10.1007/BF00142477).
- 1056 Mukherjee, A., Shankar, D., Fernando, V., Amol, P., Aparna, S.G., Fernandes,  
R., Michael, G.S., Khalap, S.T., Satelkar, N.P., Agarvadekar,  
1058 Y., Gaonkar, M.G., Tari, A.P., Kankonkar, A., Vernekar, S., 2014. Observed seasonal and intraseasonal variability of the East India Coastal  
1060 Current on the continental slope. *J. Earth Syst. Sci.* 123, 1197–1232.  
[10.1007/s12040-014-0471-7](https://doi.org/10.1007/s12040-014-0471-7).
- 1062 Mukhopadhyay, S., Shankar, D., Aparna, S.G., Mukherjee, A., 2017. Observations of the sub-inertial, near-surface East India Coastal Current. *Cont.*  
1064 *Shelf Res.* 148, 159–177. [10.1016/j.csr.2017.08.020](https://doi.org/10.1016/j.csr.2017.08.020).
- 1066 Mukhopadhyay, S., Shankar, D., Aparna, S.G., Mukherjee, A., Fernando,  
V., Kankonkar, A., Khalap, S., Satelkar, N.P., Gaonkar, M.G., Tari, A.P.,  
Khedkar, R.R., Ghatkar, S., 2020. Observed variability of the East India  
1068 Coastal Current on the continental slope during 2009–2018. *J. Earth Syst. Sci.* 129, 1–22. [10.1007/s12040-020-1346-8](https://doi.org/10.1007/s12040-020-1346-8).

- 1070 Nair, K.K.C., Madhupratap, M., Gopalakrishnan, T.C., Haridas, P., Gauns,  
M., 1999. The Arabian Sea: physical environment, zooplankton and myc-  
1072 tophid abundance. Indian J. Mar. Sci. 28, 138–145. [nopr.niscpr.res.in/handle/123456789/25690](http://nopr.niscpr.res.in/handle/123456789/25690).
- 1074 Nair, P.V., 1970. Primary productivity in the Indian seas. CMFRI Bulletin  
22, 1–63. [eprints.cmfri.org.in/id/eprint/610](http://eprints.cmfri.org.in/id/eprint/610).
- 1076 Naqvi, S.W.A., Narvekar, P.V., Desa, E., 2006. Coastal biogeochemical pro-  
cesses in the north Indian Ocean. Coastal segment (14°S–W), in: Robin-  
1078 son, A.R., Brink, K.H. (Eds.), The Sea. John Wiley and Sons, Inc. vol-  
ume 14. chapter 19, pp. 723–781.
- 1080 Naqvi, S.W.A., Noronha, R.J., Somasundar, K., Gupta, R.S., 1990. Sea-  
sonal changes in the denitrification regime of the Arabian Sea. Deep-Sea  
1082 Research 37, 593–611. [10.1016/0198-0149\(90\)90092-A](https://doi.org/10.1016/0198-0149(90)90092-A).
- Nie, L., Li, J., Wu, H., Zhang, W., Tian, Y., Liu, Y., Sun, P., Ye, Z., Ma, S.,  
1084 Gao, Q., 2023. The influence of ocean processes on fine-scale changes in  
the Yellow Sea cold water mass boundary area structure based on acoustic  
1086 observations. Rem. Sens. 15, 4272. [10.3390/rs15174272](https://doi.org/10.3390/rs15174272).
- 1088 Ohman, M.D., Hirche, H.J., 2001. Density-dependent mortality in an  
oceanic copepod population. Nature 412, 638–641. [10.1038/35088068](https://doi.org/10.1038/35088068).
- Piontkovski, S.A., Williams, R., Melnik, T.A., 1995. Spatial heterogene-  
1090 ity, biomass and size structure of plankton of the Indian Ocean: some  
general trends. Mar. Ecol. Prog. Ser. , 219–227 [www.jstor.org/stable/44634833](http://www.jstor.org/stable/44634833).

- Potiris, E., Frangoulis, C., Kalampokis, A., Ntoumas, M., Pettas, M., Peti-  
1094 hakis, G., Zervakis, V., 2018. Acoustic doppler current profiler observa-  
tions of migration patternsof zooplankton in the Cretan Sea. *Ocean Sci.*  
1096 14, 783–800. [10.5194/os-14-783-2018](https://doi.org/10.5194/os-14-783-2018).
- Prasad, T., Bahulayan, N., 1996. Mixed layer depth and thermocline clima-  
1098 tology of the Arabian Sea and western equatorial Indian Ocean. *Indian J.*  
*Mar. Sci.* 25, 189–194. [nopr.niscpr.res.in/handle/123456789/37119](https://nopr.niscpr.res.in/handle/123456789/37119).
- 1100 Qasim, S.Z., 1977. Biological productivity of the Indian Ocean. *Indian J.*  
*Mar. Sci.* 6, 122–137. [nopr.niscpr.res.in/handle/123456789/39365](https://nopr.niscpr.res.in/handle/123456789/39365).
- 1102 Quéré, C.L., Andrew, R.M., Canadell, J.G., Sitch, S., Korsbakken, J.I.,  
Peters, G.P., Manning, A.C., Boden, T.A., Tans, P.P., Houghton, R.A.,  
1104 2016. Global carbon budget 2016. *Earth Syst. Sci. Data* 8, 605–649.  
[10.5194/essd-8-605-2016](https://doi.org/10.5194/essd-8-605-2016).
- 1106 Ramamurthy, S., 1965. Studies on the plankton of the North Kanara coast  
in relation to the pelagic fishery. *J. Mar. Biol. Assoc. India* 7, 127–149.  
1108 [eprints.cmfri.org.in/id/eprint/894](https://eprints.cmfri.org.in/id/eprint/894).
- Rehim, M., Imran, M., 2012. Dynamical analysis of a delay model of  
1110 phytoplankton-zooplankton interaction. *Appl. Math. Model.* 36, 638–647.  
[10.1016/j.apm.2011.07.018](https://doi.org/10.1016/j.apm.2011.07.018).
- 1112 Rippeth, T.P., Simpson, J.H., 1998. Diurnal signals in vertical motions  
on the Hebridean shelf. *Limnol. Oceanogr.* 43, 1690–1696. [10.4319/lo.1998.43.7.1690](https://doi.org/10.4319/lo.1998.43.7.1690).
- Rochford, D., 1964. Salinity maxima in the upper 1000 metres of the north

- 1116 Indian Ocean. Marine and Freshwater Research 15, 1–24. 10.1071/  
MF9640001.
- 1118 Ryther, J.H., Hall, J.R., Pease, A.K., Bakun, A., Jones, M.M., 1966.  
Primary organic production in relation to the chemistry and hydrogra-  
1120 phy of the western Indian Ocean. Limnol. and Oceanogr. 11, 371–380.  
10.4319/lo.1966.11.3.0371.
- 1122 Saji, N.H., Goswami, B.N., Vinayachandran, P.N., Yamagata, T., 1999. A  
dipole mode in the tropical Indian Ocean. Nature 401, 360–363. 10.1038/  
1124 43854.
- 1126 Schmidt, H., Czeschel, R., Visbeck, M., 2020. Seasonal variability of the  
Arabian Sea intermediate circulation and its impact on seasonal changes  
of the upper oxygen minimum zone. Ocean Sci. 16, 1459–1474. 10.5194/  
1128 os-16-1459-2020.
- 1130 Shankar, D., 2000. Seasonal cycle of sea level and currents along the coast  
of India. Current Science 78, 279–288.
- 1132 Shankar, D., Remya, R., Anil, A.C., Vijith, V., 2019. Role of physical  
processes in determining the nature of fisheries in the eastern Arabian  
Sea. Prog. Oceanogr. 172, 124–158. 10.1016/j.pocean.2018.11.006.
- 1134 Shankar, D., Remya, R., Vinayachandran, P.N., Chatterjee, A., Behera, A.,  
2016. Inhibition of mixed-layer deepening during winter in the north-  
1136 eastern Arabian Sea by the West India Coastal Current. Clim. Dyn. 47,  
1049–1072. 10.1007/s00382-015-2888-3.
- 1138 Shankar, D., Shenoi, S.S.C., Nayak, R.K., Vinayachandran, P.N., Nam-  
poothiri, G., Almeida, A.M., Michael, G.S., Kumar, M.R.R., Sun-

<sup>1140</sup> dar, D., Sreejith, O.P., 2005. Hydrography of the eastern Arabian Sea during summer monsoon 2002. *J. Earth Syst. Sci.* 114, 459–474.  
<sup>1142</sup> 10.1007/BF02702023.

<sup>1144</sup> Shankar, D., Shetye, S.R., 1997. On the dynamics of the Lakshadweep high and low in the southeastern Arabian Sea. *J. Geophys. Res. Oceans* 102, 12551–12562. 10.1029/97JC00465.

<sup>1146</sup> Shankar, D., Vinayachandran, P., Unnikrishnan, A., 2002. The monsoon currents in the north Indian Ocean. *Prog. in ocean.* 52, 63–120. 10.1016/S0079-6611(02)00024-1.

<sup>1150</sup> Shenoi, S.S.C., Shankar, D., Michael, G.S., Kurian, J., Varma, K.K., Kumar, M.R.R., Almeida, A.M., Unnikrishnan, A.S., Fernandes, W., Barreto, N., Gnanaseelan, C., Mathew, R., Praju, K.V., Mahale, V., 2005. Hydrography and water masses in the southeastern Arabian Sea during March–June 2003. *J. Earth Syst. Sci.* 114, 475–491. 10.1007/BF02702024.

<sup>1154</sup> Shenoi, S.S.C., Shankar, D., Shetye, S.R., 2004. Remote forcing annihilates barrier layer in southeastern Arabian Sea. *Geophys. Res. Lett.* 10.1029/  
<sup>1156</sup> 2003GL019270.

<sup>1158</sup> Shetye, S.R., Gouveia, A.D., Shenoi, S.S.C., 1992. Does winter cooling lead to the subsurface salinity minimum off Saurashtra, India? *Oceanogr. Indian Ocean*, 617–625drs.nio.org/drs/bitstream/2264/  
<sup>1160</sup> 3139/2/Oceanogr\_Indian\_Ocean\_1992\_617.pdf.

<sup>1162</sup> Shetye, S.R., Gouveia, A.D., Shenoi, S.S.C., Michael, G.S., Sundar, D., Almeida, A.M., Santanam, K., 1991. The coastal current off western

- India during the northeast monsoon. Deep-Sea Res. Part A. Oceanogr.  
1164 Res. Pap. 38, 1517–1529. [10.1016/0198-0149\(91\)90087-V](https://doi.org/10.1016/0198-0149(91)90087-V).
- Shetye, S.R., Gouveia, A.D., Shenoi, S.S.C., Sundar, D., Michael, G.S.,  
1166 Almeida, A., Santanam, K., 1990. Hydrography and circulation off the  
west coast of India during the southwest monsoon 1987. J. Mar. Res. 48,  
1168 359–378.
- Shi, W., Wang, M., 2022. Phytoplankton biomass dynamics in the Arabian  
1170 Sea from VIIRS observations. J. Mar. Syst. 227, 103670. [10.1016/j.jmarsys.2021.103670](https://doi.org/10.1016/j.jmarsys.2021.103670).
- Sikka, D.R., 1980. Some aspects of the large scale fluctuations of summer monsoon rainfall over India in relation to fluctuations in the planetary and regional scale circulation parameters. Proceedings of the Indian Academy of Sciences (Earth and Planetary Sciences) 89, 179–195.  
1172 [10.1007/BF02913749](https://doi.org/10.1007/BF02913749).
- Smeti, H., Pagano, M., Menkes, C., Dhaussy, A.L., Hunt, B.P.V., Allain, V.,  
1174 Rodier, M., De Boissieu, F., Kestenare, E., Sammari, C., 2015. Spatial and temporal variability of zooplankton off New Caledonia (Southwestern Pacific) from acoustics and net measurements. J. Geophys. Res. Oceans 120, 2676–2700. [10.1002/2014JC010441](https://doi.org/10.1002/2014JC010441).
- Smith, S.L., Madhupratap, M., 2005. Mesozooplankton of the Arabian Sea: patterns influenced by seasons, upwelling, and oxygen concentrations.  
1176 Prog. Oceanogr. 65, 214–239. [10.1016/j.pocean.2005.03.007](https://doi.org/10.1016/j.pocean.2005.03.007).
- Sreenivas, P., Patnaik, K.V.K.R.K., Prasad, K.V.S.R., 2008. Monthly vari-

- 1186 ability of mixed layer over Arabian Sea using ARGO data. Mar. Geod.  
31, 17–38. 10.1080/01490410701812311.
- 1188 Subrahmanyam, R., 1959. Studies on the phytoplankton of the west coast of  
India: Part II. Physical and chemical factors influencing the production  
1190 of phytoplankton, with remarks on the cycle of nutrients and on the re-  
lationship of the phosphate-content to fish landings, in: Proc. Ind. Acad.  
1192 Sci., Springer. pp. 189–252. 10.1007/BF03051925.
- 1194 Subrahmanyam, R., Sarma, A.H., 1960. Studies on the phytoplankton of the  
west coast of India. Part III. Seasonal variation of the phytoplankters and  
environmental factors. Indian J. Fish. 7, 307–336. [eprints.cmfri.org.in/1899/](http://eprints.cmfri.org.in/1899/).
- 1198 Torrence, C., Compo, G.P., 1998. A practical guide to wavelet analysis. Bull.  
Am. Meteorol. Soc. 79, 61–78. 10.1175/1520-0477(1998)079<0061:  
APGTWA>2.0.CO;2.
- 1200 Ursella, L., Cardin, V., Batistić, M., Garić, R., Gačić, M., 2018. Evidence of  
zooplankton vertical migration from continuous Southern Adriatic buoy  
1202 current-meter records. Prog. Oceanogr. 167, 78–96. 10.1016/j.pocean.  
2018.07.004.
- 1204 Ursella, L., Pensieri, S., Pallàs-Sanz, E., Herzka, S.Z., Bozzano, R., Tenreiro,  
M., Cardin, V., Candela, J., Sheinbaum, J., 2021. Diel, lunar and seasonal  
1206 vertical migration in the deep western Gulf of Mexico evidenced from  
a long-term data series of acoustic backscatter. Prog. Oceanogr. 195,  
1208 102562. 10.1016/j.pocean.2021.102562.
- Vijith, V., Shetye, S.R., Gouveia, A.D., Shenoi, S.S.C., Michael, G.S., Sun-

- 1210        dar, D., 2022. Circulation in the region of the West India Coastal Current  
in March 1994 hydrographic and altimeter data. *J. Earth Syst. Sci.* 131,  
1212        16. [10.1007/s12040-021-01761-5](https://doi.org/10.1007/s12040-021-01761-5).
- 1214        Vijith, V., Vinayachandran, P.N., Thushara, V., Amol, P., Shankar, D.,  
Anil, A.C., 2016. Consequences of inhibition of mixed-layer deepening  
by the West India Coastal Current for winter phytoplankton bloom in  
1216        the northeastern Arabian Sea. *J. Geophys. Res. Oceans* 121, 6583–6603.  
[10.1002/2016JC012004](https://doi.org/10.1002/2016JC012004).
- 1218        Wiebe, P.H., Greene, C.H., Stanton, T.K., Burczynski, J., 1990. Sound  
scattering by live zooplankton and micronekton: empirical studies with  
1220        a dual-beam acoustical system. *The Journal of the Acoustical Society of  
America* 88, 2346–2360. [10.1121/1.400077](https://doi.org/10.1121/1.400077).
- 1222        Winder, M., Schindler, D.E., 2004. Climatic effects on the phenology of lake  
processes. *Global Change Biol.* 10, 1844–1856. [10.1111/j.1365-2486.  
2004.00849.x](https://doi.org/10.1111/j.1365-2486.2004.00849.x).
- 1226        Wishner, K.F., Gowing, M.M., Gelfman, C., 1998. Mesozooplankton  
biomass in the upper 1000 m in the Arabian Sea: overall seasonal and  
geographic patterns, and relationship to oxygen gradients. *Deep-Sea Res.*  
1228        Part II Top. Stud. Oceanogr. 45, 2405–2432. [10.1016/S0967-0645\(98\)  
00078-2](https://doi.org/10.1016/S0967-0645(98)00078-2).
- 1230        Wyrtki, K., Bennett, E.B., Rochford, D.J., Expedition, I.I.O., (U.S.),  
N.S.F., of Hawaii (Honolulu), U., 1971. Oceanographic atlas of the  
1232        International Indian Ocean Expedition. National Science Foundation.  
[//cir.nii.ac.jp/crid/1130000796355741312](https://cir.nii.ac.jp/crid/1130000796355741312).

<sup>1234</sup> Yankelovich, D., 1971. Interpreting the New Life Styles. Sales Management, the Marketing Magazine, Dartnell Corporation. [https://en.wikipedia.org/wiki/McNamara\\_fallacy](https://en.wikipedia.org/wiki/McNamara_fallacy).

**Table 1:** ADCP deployment details at the respective locations are shown in this table. All ADCPs operated at 153.3 kHz with a 1 hour interval, and vertical bin size of 4 m. Moorings were deployed on the continental slope at depths of approximately 950–1200 m and serviced annually, subject to ship availability. The sixth column lists the reference echo intensity (Er) for each beam, and the seventh column provides the corresponding RSSI conversion factor (Deines, 1999).

Station (Position; °E, °N)	Date		Depth (in m)			Kc
	Deployment	Recovery	Ocean	ADCP	Er	
Okha (67.47, 22.26)	01/10/2018	01/12/2019	996	118	37 , 37 , 37 , 36	0.42 , 0.44 , 0.42 , 0.43
	01/12/2019	04/12/2020	1166	312	39 , 36 , 38 , 36	0.42 , 0.44 , 0.42 , 0.43
	04/12/2020	08/03/2022	1021	144	41 , 37 , 38 , 37	0.42 , 0.44 , 0.42 , 0.43
	08/03/2022	01/01/2023	1019	142	37 , 38 , 39 , 36	0.42 , 0.44 , 0.42 , 0.43
	01/01/2023	11/12/2023	1072	200	37 , 40 , 42 , 37	0.42 , 0.44 , 0.42 , 0.43
Mumbai (69.24, 20.01)	09/11/2017	29/09/2018	1025	150	36 , 34 , 39 , 42	0.40 , 0.40 , 0.40 , 0.40
	29/09/2018	29/11/2019	1122	125	35 , 36 , 39 , 42	0.40 , 0.40 , 0.40 , 0.40
	29/11/2019	02/12/2020	1143	164	37 , 34 , 39 , 43	0.40 , 0.40 , 0.40 , 0.40
	02/12/2020	06/03/2022	1125	142	36 , 34 , 39 , 42	0.40 , 0.40 , 0.40 , 0.40
	07/03/2022	02/01/2023	1103	158	37 , 34 , 40 , 43	0.40 , 0.40 , 0.40 , 0.40
	02/01/2023	09/12/2023	1091	944	35 , 37 , 40 , 43	0.40 , 0.40 , 0.40 , 0.40
Jaigarh (71.12, 17.53)	27/10/2017	27/09/2018	1039	198	32 , 35 , 33 , 32	0.45 , 0.45 , 0.45 , 0.45
	27/09/2018	30/10/2019	1032	164	32 , 35 , 33 , 31	0.45 , 0.45 , 0.45 , 0.45
	03/11/2019	30/11/2020	1142	264	32 , 36 , 33 , 32	0.45 , 0.45 , 0.45 , 0.45
	30/11/2020	05/03/2022	1099	119	33 , 36 , 34 , 32	0.45 , 0.45 , 0.45 , 0.45
Goa (72.74, 15.17)	03/10/2017	25/09/2018	1000	174	35 , 37 , 34 , 35	0.44 , 0.44 , 0.40 , 0.41
	25/09/2018	16/10/2019	969	145	38 , 36 , 36 , 34	0.44 , 0.44 , 0.40 , 0.41
	16/10/2019	29/11/2020	966	143	44 , 38 , 36 , 43	0.44 , 0.44 , 0.40 , 0.41
	29/11/2020	03/03/2022	985	157	35 , 40 , 35 , 38	0.44 , 0.44 , 0.40 , 0.41
	03/03/2022	05/01/2023	984	159	35 , 38 , 35 , 34	0.44 , 0.44 , 0.40 , 0.41
	05/01/2023	14/12/2023	996	195	36 , 38 , 36 , 35	0.44 , 0.44 , 0.4 , 0.41
Udupi (74.04, 12.5)	05/10/2017	06/10/2018	1028	176	44 , 46 , 29 , 35	0.45 , 0.45 , 0.45 , 0.45
	06/10/2018	18/10/2019	1027	179	32 , 38 , 30 , 36	0.45 , 0.45 , 0.45 , 0.45
	18/10/2019	11/12/2020	1018	168	33 , 37 , 31 , 38	0.45 , 0.45 , 0.45 , 0.45
	11/03/2022	06/01/2023	1036	155	31 , 32 , 32 , 33	0.45 , 0.45 , 0.45 , 0.45
	06/01/2023	15/12/2023	1035	882	31 , 33 , 32 , 34	0.45 , 0.45 , 0.45 , 0.45
Kollam (75.44, 9.05)	07/10/2017	08/10/2018	1174	200	43 , 55 , 45 , 43	0.49 , 0.50 , 0.49 , 0.50
	08/10/2018	20/10/2019	1160	123	49 , 62 , 46 , 46	0.49 , 0.50 , 0.49 , 0.50
	20/10/2019	13/12/2020	1209	176	52 , 61 , 54 , 55	0.49 , 0.50 , 0.49 , 0.50
	13/12/2020	13/03/2022	1129	91	49 , 51 , 46 , 47	0.49 , 0.50 , 0.49 , 0.50
	13/03/2022	08/01/2023	1149	164	41 , 48 , 43 , 41	0.49 , 0.50 , 0.49 , 0.50
	08/01/2023	17/12/2023	1171	987	41 , 45 , 43 , 41	0.49 , 0.50 , 0.49 , 0.50
Kanyakumari (77.39, 6.96)	08/10/2017	10/10/2018	1055	181	32 , 34 , 38 , 35	0.45 , 0.45 , 0.45 , 0.45
	10/10/2018	22/10/2019	1075	180	36 , 34 , 39 , 36	0.45 , 0.45 , 0.45 , 0.45
	22/10/2019	14/12/2020	1060	167	33 , 35 , 36 , 35	0.45 , 0.45 , 0.45 , 0.45
	14/12/2020	14/03/2022	1184	287	34 , 36 , 36 , 35	0.45 , 0.45 , 0.45 , 0.45

**Table 2:** Volumetric zooplankton samples collected from various stations. Sampling depths were standardized in later years to the following depth ranges: 0–25 m, 25–50 m, 50–75 m, 75–100 m, and 100–150 m. Abbreviations: Okha (O), Mumbai (M), Jaigarh (J), Goa (G), Udupi (U), Kollam (K), Kanyakumari (KK); numeric tags denote specific station cruises.

Sample number	Tag	Lat ( $^{\circ}$ N)	Lon ( $^{\circ}$ E)	Date	Time (IST)	Sampling depth range (m)
1-3	G1	15.18	72.79	25 Sep 18	0452	50 – 25, 100 – 50, 150 – 100
4-6	G2	15.16	72.71	25 Sep 18	2108	50 – 25, 100 – 50, 150 – 100
7-10	G2	15.16	72.71	25 Sep 18	2137	40 – 20, 60 – 40, 80 – 60, 100 – 80
11-14	J1	–	–	26 Sep 18	2000	40 – 20, 60 – 40, 80 – 60, 100 – 80
15-17	J2	–	–	27 Sep 18	2000	50 – 25, 100 – 50, 150 – 100
18-21	J2	–	–	27 Sep 18	2100	40 – 20, 60 – 40, 80 – 60, 100 – 80
22-25	M1	20.00	69.19	28 Sep 18	2135	40 – 20, 60 – 40, 80 – 60, 100 – 80
26-27	M1	20.00	69.19	28 Sep 18	2205	50 – 25, 100 – 50
28-29	M2	20.01	69.20	29 Sep 18	2035	50 – 25, 100 – 50
30-33	M2	20.01	69.20	29 Sep 18	2057	40 – 20, 60 – 40, 80 – 60, 100 – 80
34-37	U1	–	–	5 Oct 18	2000	40 – 20, 60 – 40, 80 – 60, 100 – 80
38-40	U1	–	–	5 Oct 18	2100	50 – 25, 100 – 50, 150 – 100
41-43	U2	–	–	6 Oct 18	2000	50 – 25, 100 – 50, 150 – 100
44-47	U2	–	–	6 Oct 18	2100	40 – 20, 60 – 40, 80 – 60, 100 – 80
48-51	K1	9.06	75.42	8 Oct 18	0421	40 – 20, 60 – 40, 80 – 60, 100 – 80
52-54	K1	9.06	75.42	8 Oct 18	0449	50 – 25, 100 – 50, 150 – 100
55-56	K2	9.04	75.40	8 Oct 18	2027	50 – 25, 100 – 50
57-60	K2	9.04	75.40	8 Oct 18	2045	40 – 20, 60 – 40, 80 – 60, 100 – 80
61-64	G2	15.16	72.74	16 Oct 19	0829	50 – 25, 75 – 50, 100 – 75, 150 – 100
65-67	G3	15.16	72.74	16 Oct 19	1812	50 – 25, 75 – 50, 100 – 75
68-70	K2	9.02	75.42	20 Oct 19	0840	50 – 25, 75 – 50, 100 – 75
71-74	K3	9.04	75.43	20 Oct 19	1934	50 – 25, 75 – 50, 100 – 75, 150 – 100
75-78	KK1	–	–	22 Oct 19	0742	50 – 25, 75 – 50, 100 – 75, 150 – 100
79-82	KK2	–	–	22 Oct 19	1925	50 – 25, 75 – 50, 100 – 75, 150 – 100
83-86	J1	–	–	30 Oct 19	0324	50 – 25, 75 – 50, 100 – 75, 150 – 100
87-89	J2	–	–	4 Nov 19	0946	75 – 50, 100 – 75, 150 – 100
90-92	M2	19.98	69.22	29 Nov 19	1434	50 – 25, 75 – 50, 100 – 75
93-96	M3	20.01	69.23	30 Nov 19	0958	50 – 25, 75 – 50, 100 – 75, 150 – 100
97-100	O1	22.24	67.49	1 Dec 19	0937	50 – 25, 75 – 50, 100 – 75, 150 – 100
101	O2	22.25	67.46	1 Dec 19	1957	150 – 100
102-105	G3	15.68	73.22	28 Nov 20	0930	50 – 25, 75 – 50, 100 – 75, 150 – 100
105-108	G4	15.32	73.22	29 Nov 20	1558	50 – 25, 75 – 50, 100 – 75, 150 – 100
108-110	J2	17.85	71.21	30 Nov 20	1458	75 – 50, 100 – 75, 150 – 100
111-114	J3	17.91	71.21	1 Dec 20	1052	50 – 25, 75 – 50, 100 – 75, 150 – 100
115-118	M4	20.03	69.38	2 Dec 20	2016	50 – 25, 75 – 50, 100 – 75, 150 – 100
119	O2	22.41	67.80	4 Dec 20	0953	150 – 100
120-123	O3	22.41	67.79	4 Dec 20	2011	50 – 25, 75 – 50, 100 – 75, 150 – 100
124-127	K3	9.11	75.72	12 Dec 20	2335	50 – 25, 75 – 50, 100 – 75, 150 – 100
128-131	K4	9.06	75.74	13 Dec 20	1507	50 – 25, 75 – 50, 100 – 75, 150 – 100
132-134	KK1	7.62	77.63	14 Dec 20	1226	50 – 25, 75 – 50
135-138	KK2	7.62	77.63	14 Dec 20	2047	50 – 25, 75 – 50, 100 – 75, 150 – 100
139-142	G4	15.32	73.21	3 Mar 22	0823	50 – 25, 75 – 50, 100 – 75, 150 – 100
143-146	G5	15.68	73.21	4 Mar 22	1030	50 – 25, 75 – 50, 100 – 75, 150 – 100
147-150	M5	19.99	69.23	7 Mar 22	0957	50 – 25, 75 – 50, 100 – 75, 150 – 100
151-154	O3	22.24	67.50	8 Mar 22	0806	50 – 25, 75 – 50, 100 – 75, 150 – 100
155-158	U3	12.50	74.04	12 Mar 22	1156	50 – 25, 75 – 50, 100 – 75, 150 – 100

159-160	K4	9.04	75.42	13 Mar 22	1027	$50 - 25, 75 - 50, 100 - 75$
165-168	G7	–	–	5 Jan 23	1935	$50 - 25, 75 - 50, 100 - 75, 150 - 100$
169-172	J4	–	–	4 Jan 23	1134	$50 - 25, 75 - 50, 100 - 75, 150 - 100$
173-176	M6	–	–	2 Jan 23	1950	$50 - 25, 75 - 50, 100 - 75, 150 - 100$
177-180	U4	–	–	6 Jan 23	1538	$50 - 25, 75 - 50, 100 - 75, 150 - 100$
181-184	K5	–	–	8 Jan 23	1156	$50 - 25, 75 - 50, 100 - 75, 150 - 100$

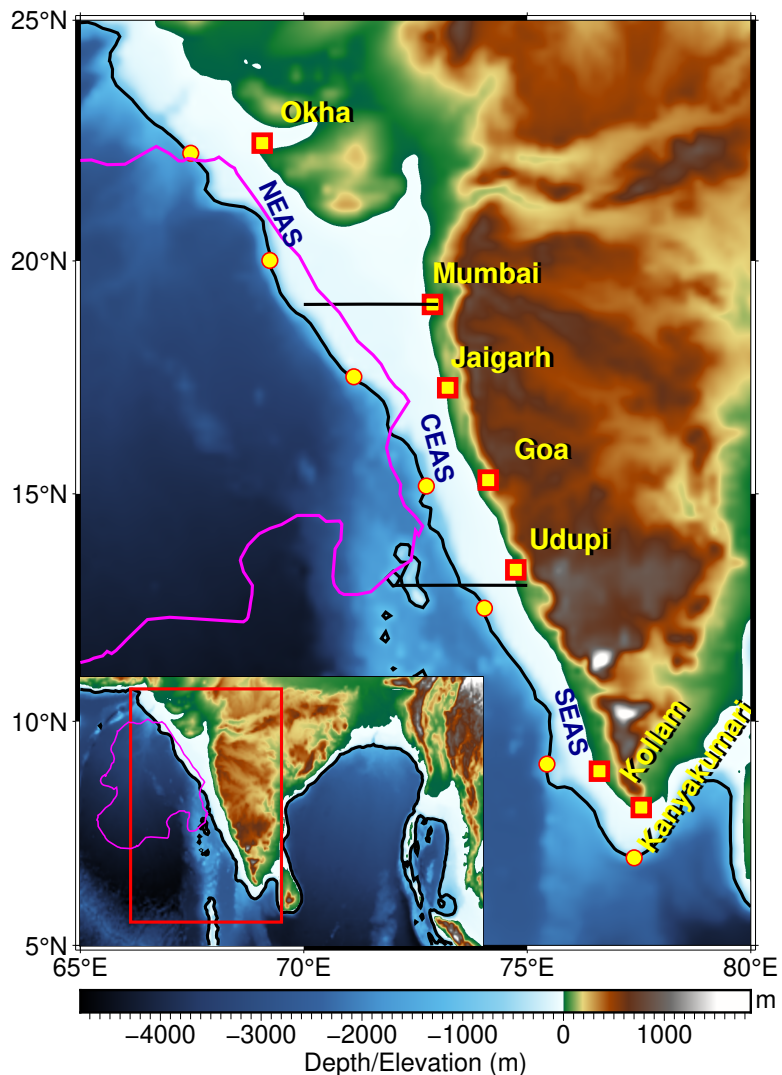


**Figure 1:** The map illustrates the study region in the eastern Arabian Sea (EAS), where slope moorings are positioned along the ~1000 m isobath, as shown by black bathymetry contour. The continental shelf widens progressively toward the north along the Indian west coast. Mooring locations off Okha and Mumbai are situated in the northeastern Arabian Sea (NEAS), those off Jaigarh and Goa in the central Arabian Sea (CEAS), and those off Kollam and Kanyakumari in the southeastern Arabian Sea (SEAS). Udupi lies just north of the boundary separating the CEAS and SEAS. The oxygen minimum zone (OMZ) is outlined by magenta contours, following A22 (Naqvi et al., 1990; Smith and Madhupratap, 2005).

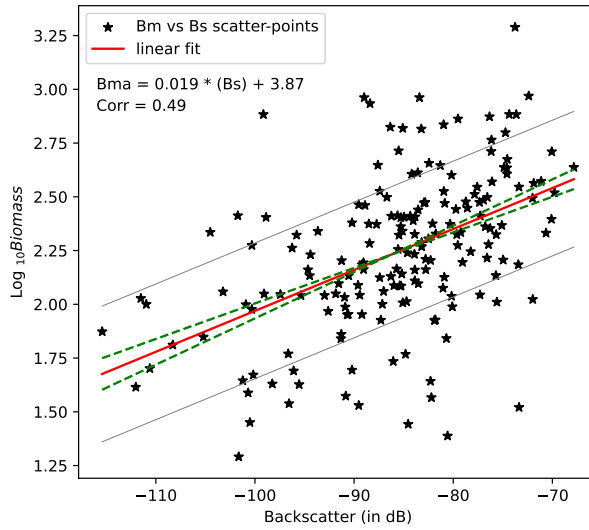


**Figure 2:** A linear regression between biomass (log<sub>10</sub> scale) and acoustic backscatter strength (in dB) is presented. The regression falls within the uncertainty bounds reported by A22, who used 67 data points. The present analysis uses an expanded dataset of 184 points, incorporating additional volumetric zooplankton samples. Bs is ADCP backscatter, and Bma is zooplankton biomass derived from the former. The best-fit equation is  $Bma = 0.019 Bs + 3.87$ , with a correlation coefficient of 0.49. The  $\pm 1$  SD of linear regressed line shown in parallel grey lines. Dashed green lines denote the uncertainty in slope and intercept estimates, corresponding to an approximate biomass uncertainty of  $\sim 14 \text{ mg m}^{-3}$ . The SD in log<sub>10</sub>(biomass) is  $\pm 0.49$ , translating to a backscatter range of 48.58 dB. This range spans the full extent of observed backscatter values, supporting the reliability of using ADCP-derived backscatter as a proxy for zooplankton biomass.

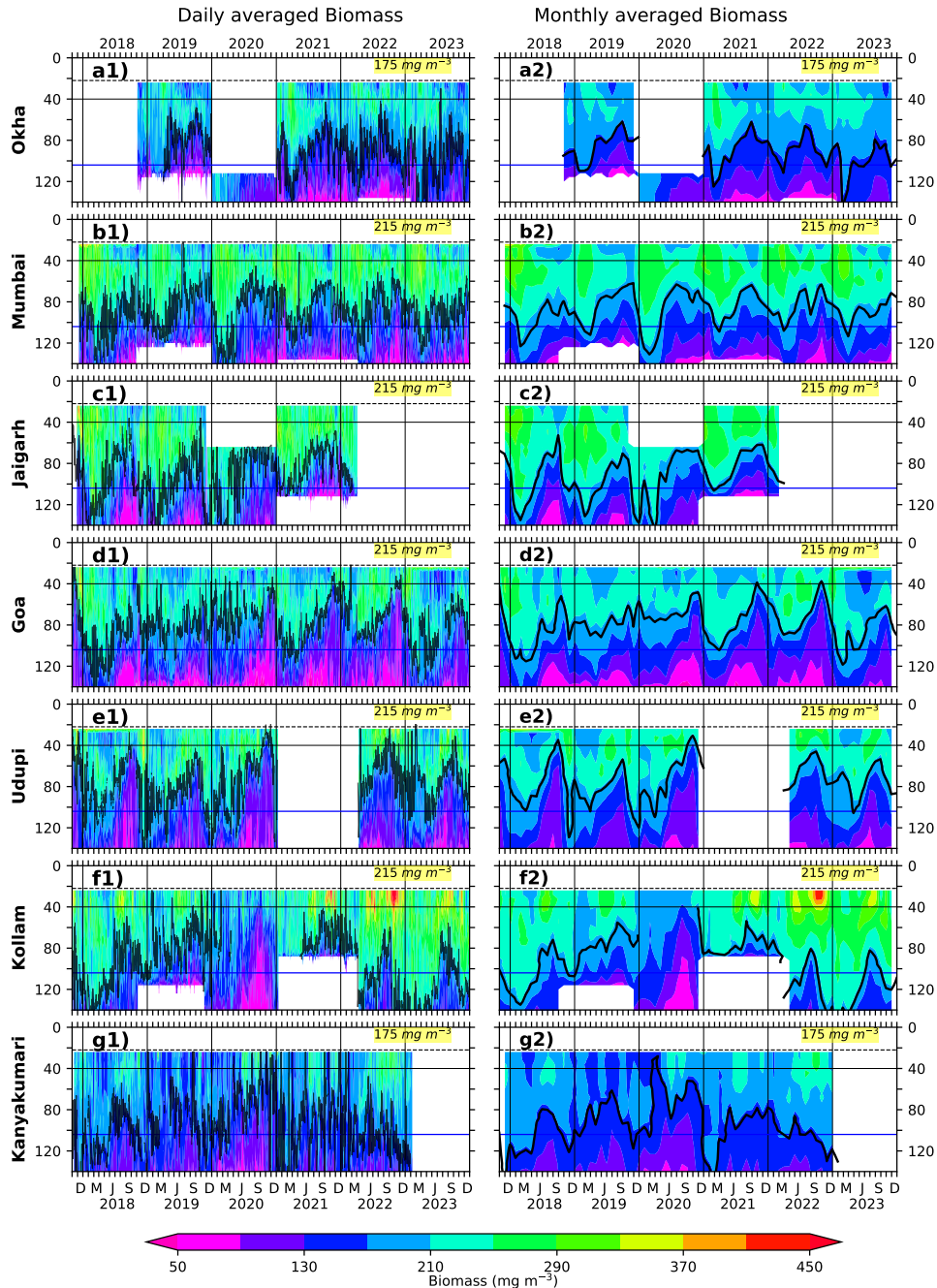


**Figure 3:** Daily and monthly averaged biomass at the EAS mooring sites, from north (top) to south (bottom), are presented where the ordinate is time and abscissa is depth (in m). Black contours denote biomass levels of  $175 \text{ mg m}^{-3}$  for Okha and Kanyakumari, and  $215 \text{ mg m}^{-3}$  for the other locations. These contours are location-specific, and were chosen to optimally represent seasonal biomass variation in relation to local physico-chemical conditions. The top  $\sim 10\%$  of backscatter data<sup>58</sup>, and hence the biomass data, were excluded due to echo-induced noise. A dashed horizontal line at 22 m marks the top edge of the first ADCP bin (centered at 24 m). Vertical black lines mark year boundaries, while horizontal black and blue lines represent 40 m and 104 m depths, respectively. At Kollam in 2020, strong year-to-year variation prevents assignment of a distinctive biomass demarcating contour as compared to other years of the same location.

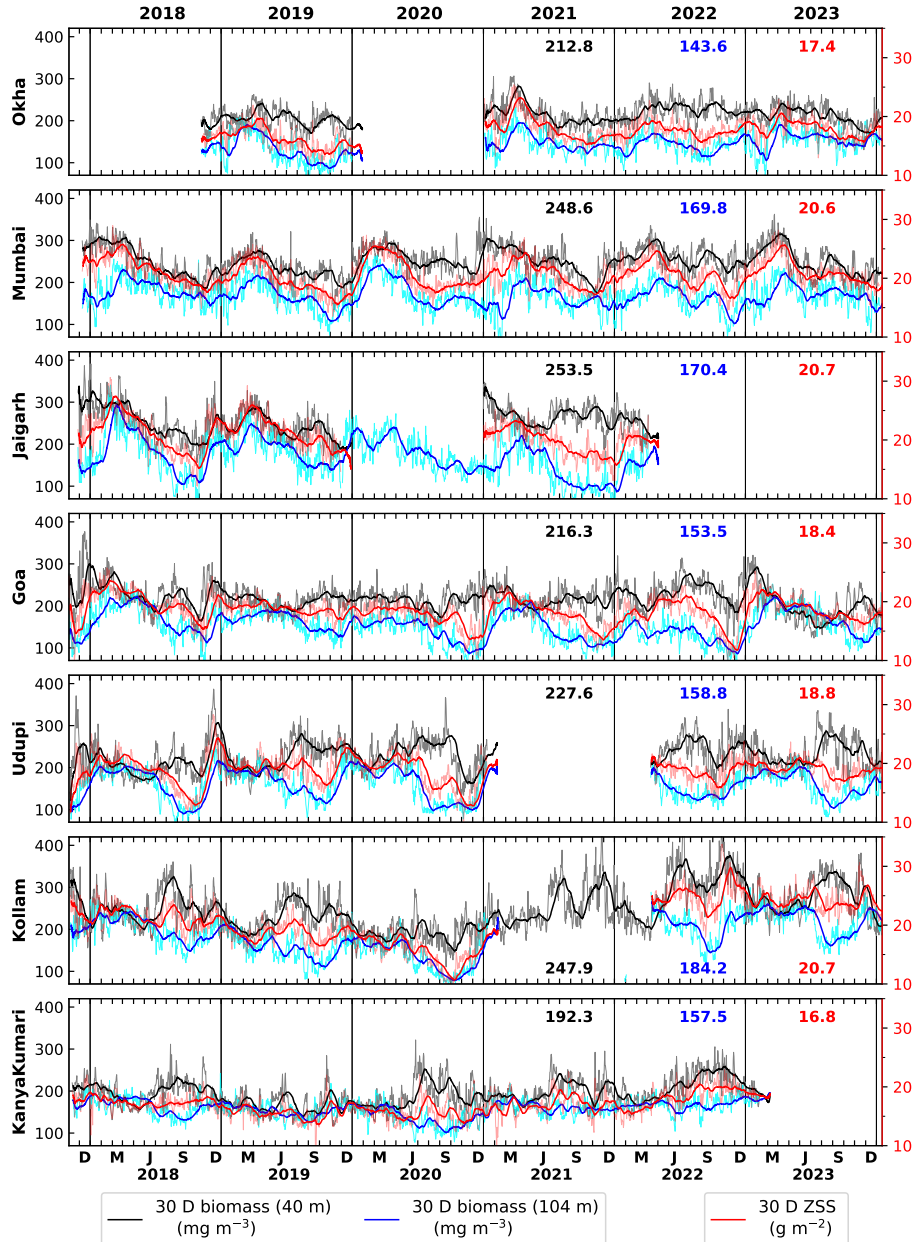


**Figure 4:** Biomass at 40 m (grey and black) and 104 m (cyan and blue), along with zooplankton standing stock (ZSS; pink and red; integrated over 24–120 m), are shown, where lighter shades represent daily values and darker shades indicate 30-day rolling averages. The biomass time series at 40 m and 104 m share a common ordinate, labeled on the left axis with units  $\text{mg m}^{-3}$ , whereas the ZSS time series uses a separate ordinate displayed on the right with units  $\text{gm m}^{-2}$ . The mean biomass at 40 m and 104 m, as well as the mean ZSS, are noted in the top-right corner using their respective color codes. Short-lived biomass spikes (appearing in the daily data) and longer-duration bursts (visible in the rolling mean) are evident, e.g., at 40 m, the spikes (bursts) typically last a few days (several days to weeks), e.g., during isolated days in June 2020 (throughout June–July 2020) off SEAS. Similar features are observed at all locations at 104 m also, though with varying magnitude.

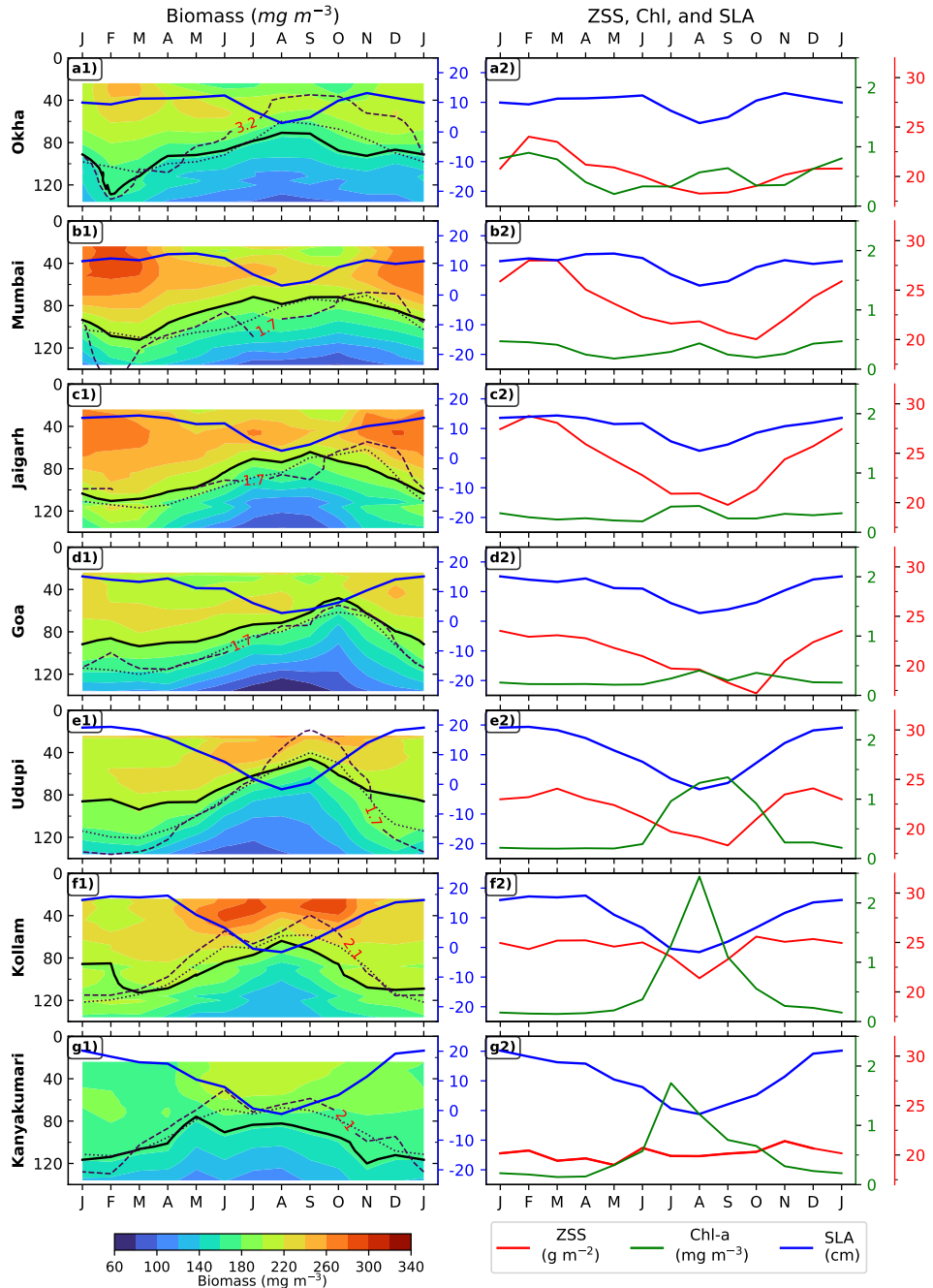


**Figure 5:** The left panels show the monthly climatology of zooplankton biomass at seven mooring locations. The D215 (D175 off Okha and Kanyakumari) are plotted as solid black lines, while the 23°C isotherm is shown as a dotted line, and oxygen concentrations are shown as dashed contours, labeled individually for each mooring, as they vary across the EAS. The right panels present the climatology of ZSS (biomass integrated over 24–140 m, derived from the climatology) and c60a at each site. The solid blue line indicates the climatological sea level anomaly (SLA), computed from data spanning October 2017 to December 2023, and is overlaid as background for each location in both left and right panels. The ordinates and labels are color coded for clarity.

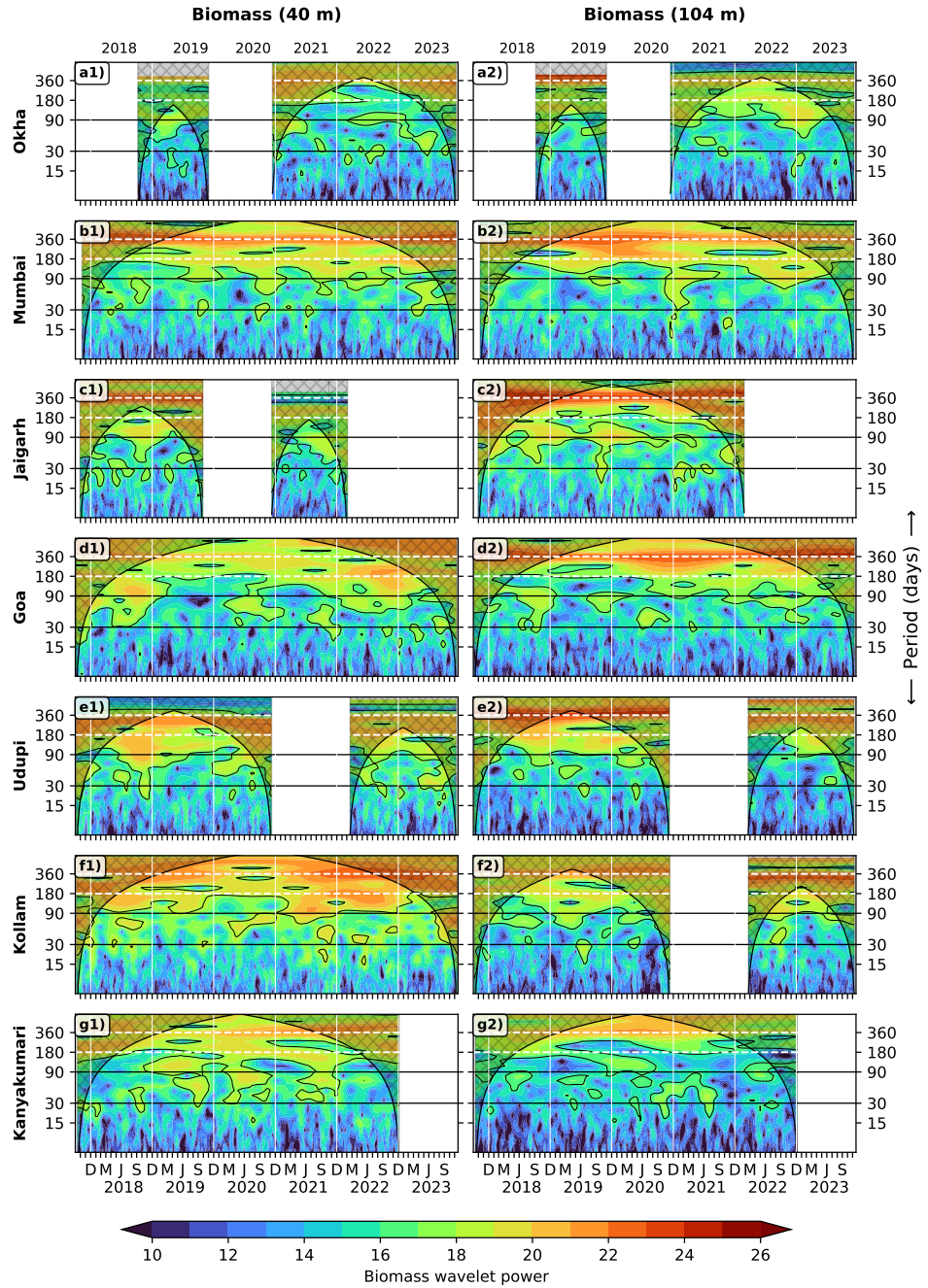


**Figure 6:** Wavelet power spectra (Morlet) of zooplankton biomass at 40 m (left panels) and 104m (right panels) for seven mooring locations in the eastern Arabian Sea, arranged from north to south. The x-axis shows time, and the y-axis shows period in days. Wavelet power and period is represented on a  $\log_2$  scale. The 95% significance level is outlined by black contours, and the solid black line marks the cone of influence, delineating the semi-transparent shaded region where edge effects become significant and power values are considered unreliable. Horizontal dashed white lines mark annual and semi-annual periods, and solid black lines contains intraseasonal band (30–90 days). Vertical white lines denote calendar year boundaries. High-power regions indicate dominant temporal scales of biomass variability across depths and sub-regions of the EAS.

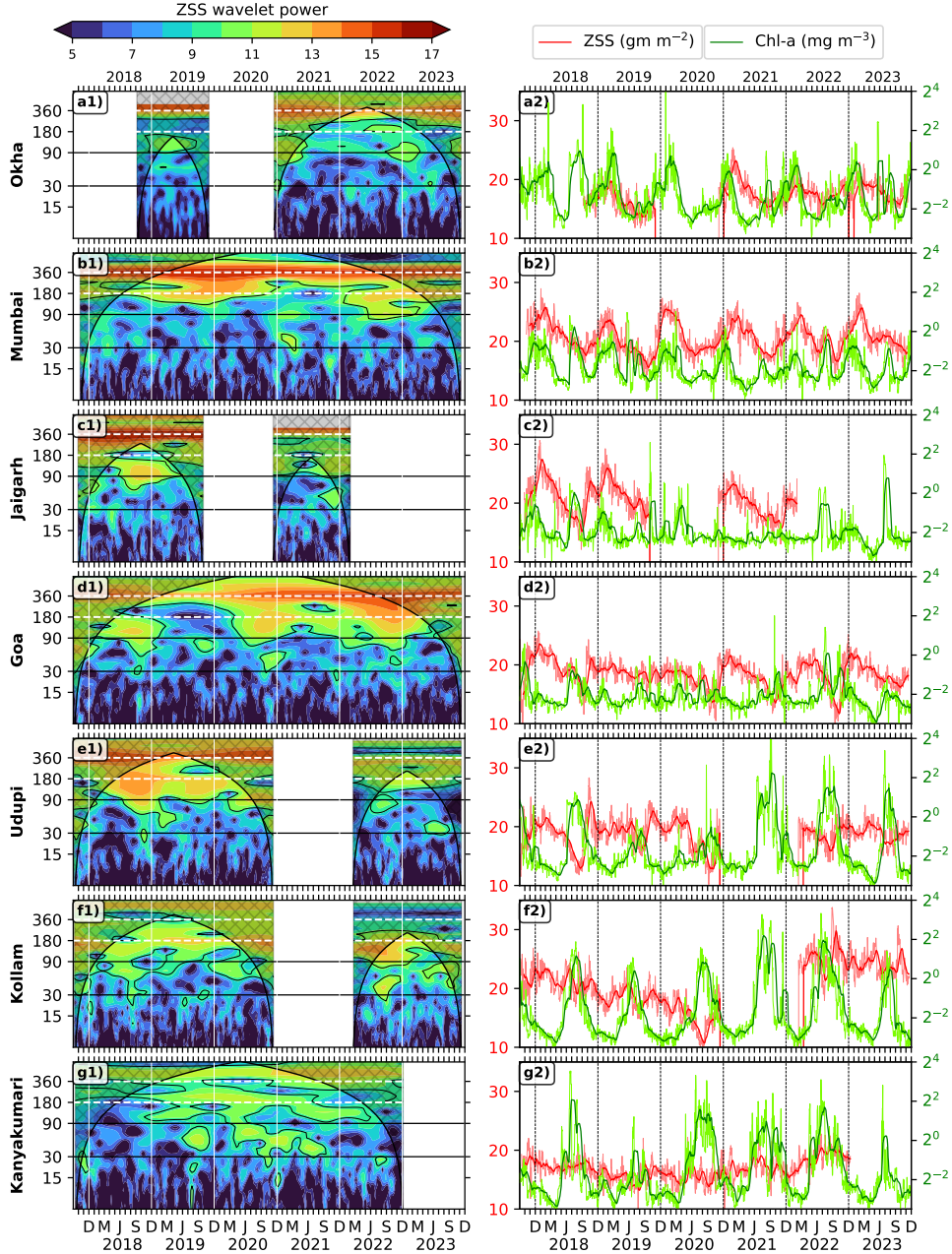


**Figure 7:** The left panel shows the wavelet power spectra (Morlet) of ZSS, with time on the x-axis and period (days) on the y-axis. Power is displayed on a  $\log_2$  scale, 95% significance level is outlined by black contours, and the solid black line marks the cone of influence, delineating the semi-transparent shaded region where power values are considered unreliable due to edge effects. Horizontal dashed white lines mark annual and semi-annual periods, and solid black lines contain intraseasonal band (30–90 days). Vertical white lines denote year boundaries. The right panel presents the time series of ZSS (biomass integrated over 24–120 m), with daily values in pink and a 30-day rolling mean in red. The rolling mean of chl-a is overlaid in solid green, with its daily values shown in light green. Rolling averages are computed if at least 25 valid ZSS values and 10 valid chl-a values are available within the 30-day window. Higher power in the annual period off Mumbai and Goa aligns with the annual signal observed at 40 and 104 m (Fig. 6).

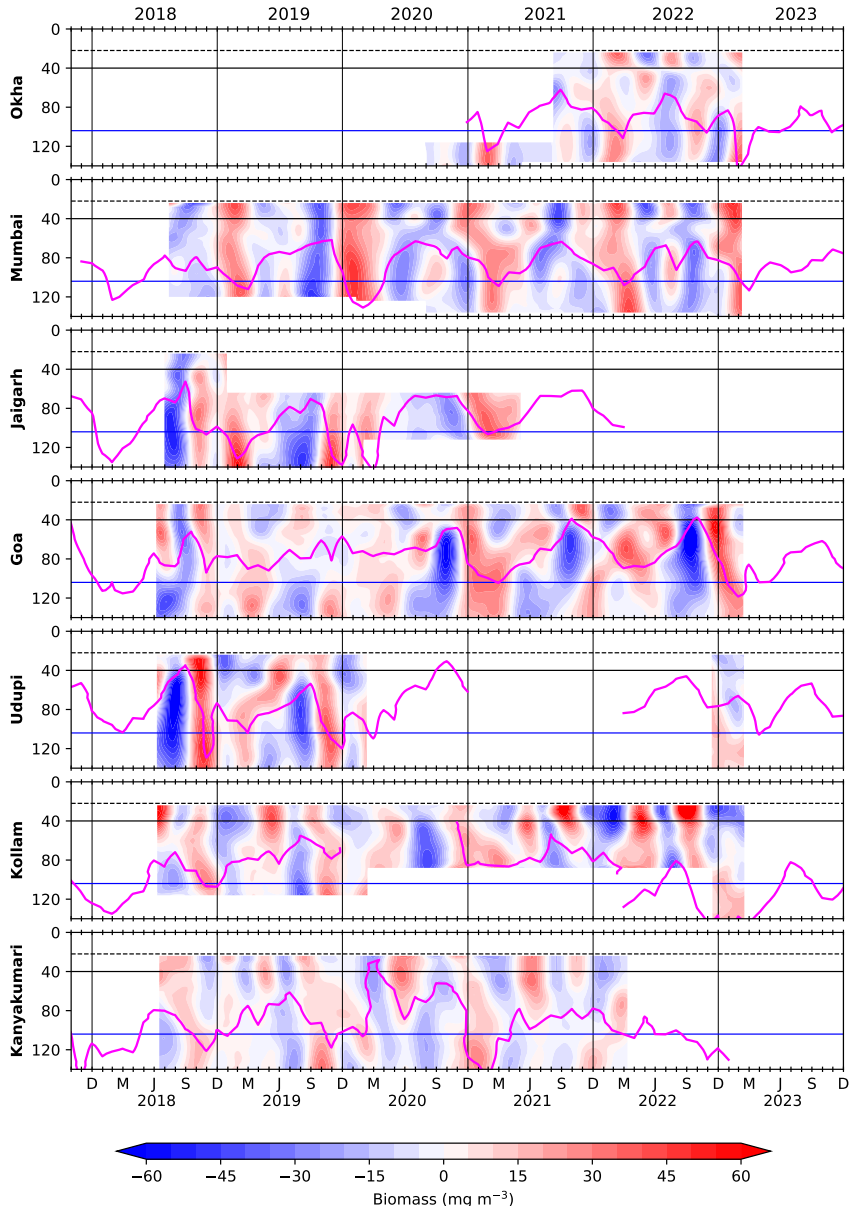


**Figure 8:** Biomass variability in the combined seasonal band (100–400 days). The seasonal band comprises: (1) annual variation associated with upwelling during the summer monsoon and downwelling during the winter monsoon, and (2) intra-annual variability driven by seasonal asymmetry. Horizontal black and blue lines indicate depths of 40 m and 104 m, respectively; vertical grey lines separate calendar years. The dashed line at 22 m marks the upper edge of the first ADCP bin (centered at 24 m). Solid magenta curves represent D215 (D175 off Okha and Kanyakumari), derived from monthly biomass climatology.

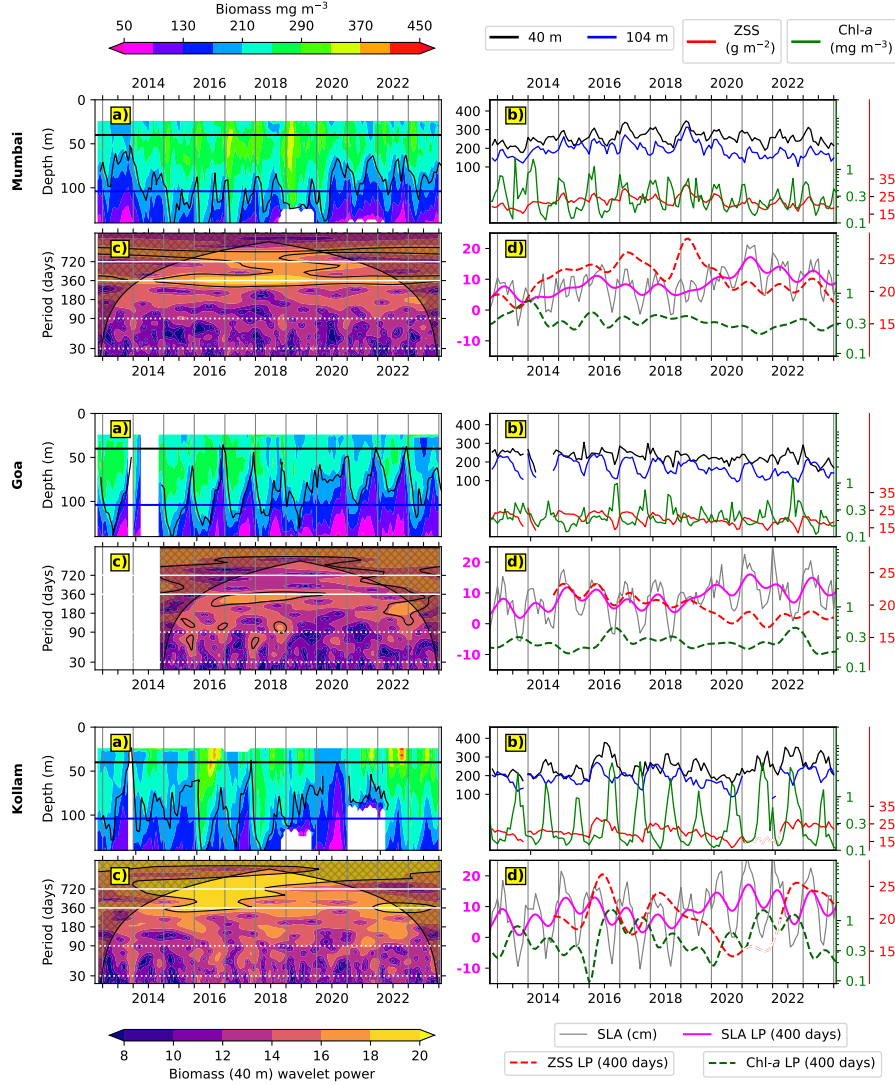


**Figure 9:** Decade-long biomass records from Mumbai, Goa, and Kollam. Each location is represented by a set of four panels. The top four panels correspond to Mumbai: (a) Time vs depth figure of biomass, with black and blue lines indicating biomass at 40 m and 104 m, respectively. Vertical grey lines denote year boundaries. (b) Time series of biomass at 40 m (black) and 104 m (blue), overlaid with ZSS (red) and chl-a (green). (c) Wavelet power spectrum of 40 m biomass, with white lines marking periodicities 720 and 360 days; dotted lines delineate the intraseasonal band (30–90 days). (d) Monthly resampled SLA (grey), overlaid with its 400-day low-pass filtered signal (magenta). Also shown are the 400-day low-pass Butterworth-filtered time series of chl-a and ZSS. All variables are resampled to a monthly time axis, and the units are: biomass (40 m and 104 m) –  $\text{mg m}^{-3}$ ; ZSS –  $\text{g m}^{-2}$ ; chl-a –  $\text{mg m}^{-3}$ ; SLA – cm. The same panel arrangement is repeated for Goa (middle set) and Kollam (bottom set). A clear biennial signal is observed off Kollam, appears weaker off Goa, but becomes more evident again off Mumbai.

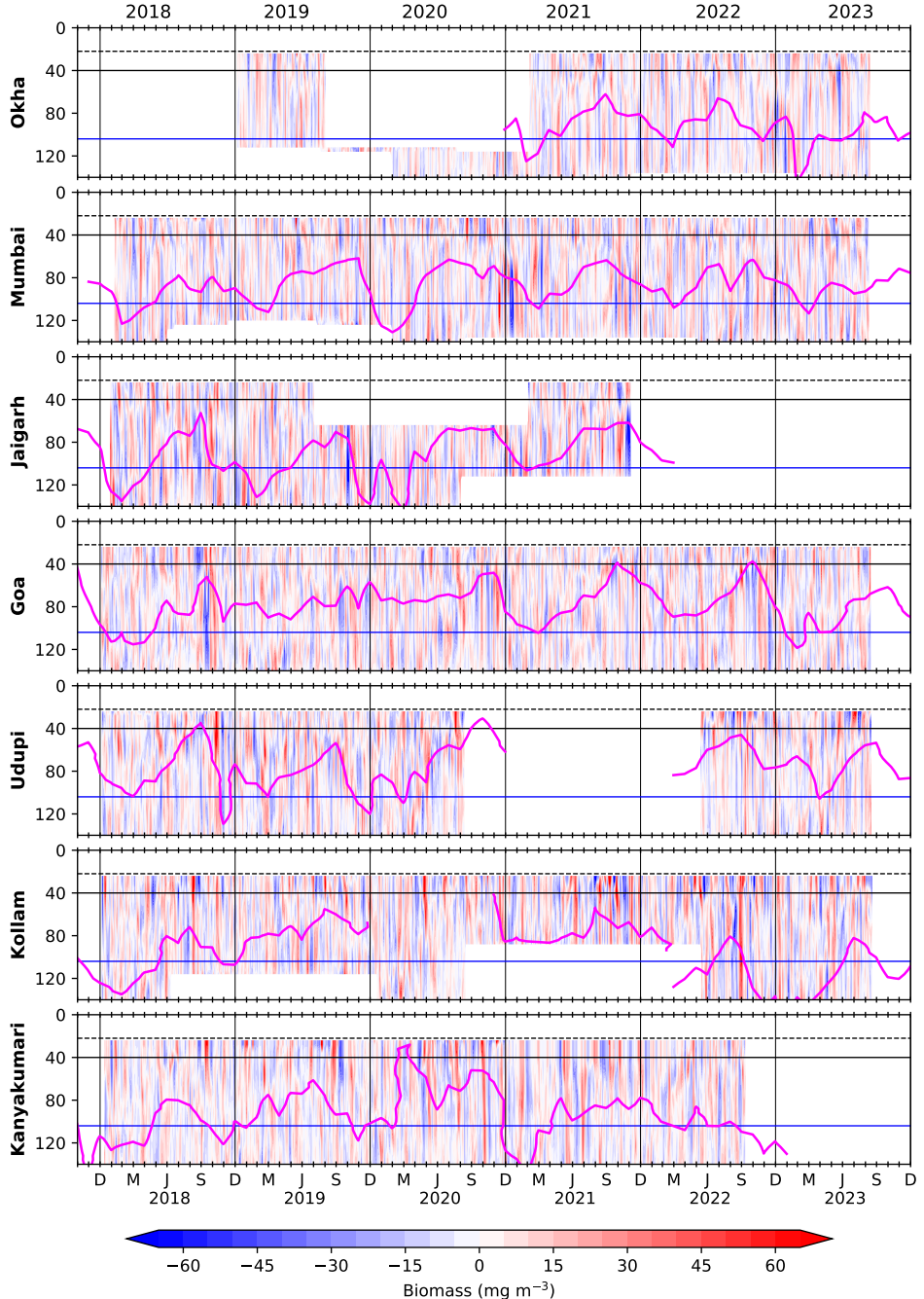


**Figure 10:** Biomass variation in the intraseasonal band (5–90 day period) is extracted using a Lanczos band-pass filter, capturing both high- and low-frequency intraseasonal components. Horizontal black and blue lines represent depths of 40 m and 104 m, respectively. Vertical black lines separate calendar years, and solid magenta curves indicate  $D215$  (or  $D175$  off Okha and Kanyakumari), derived from monthly biomass. The dashed line at 22 m marks the upper boundary of the first bin (centered at 24 m). Intraseasonal variability is evident throughout the time series and appears coherent along the slope, notably during October–December 2018.

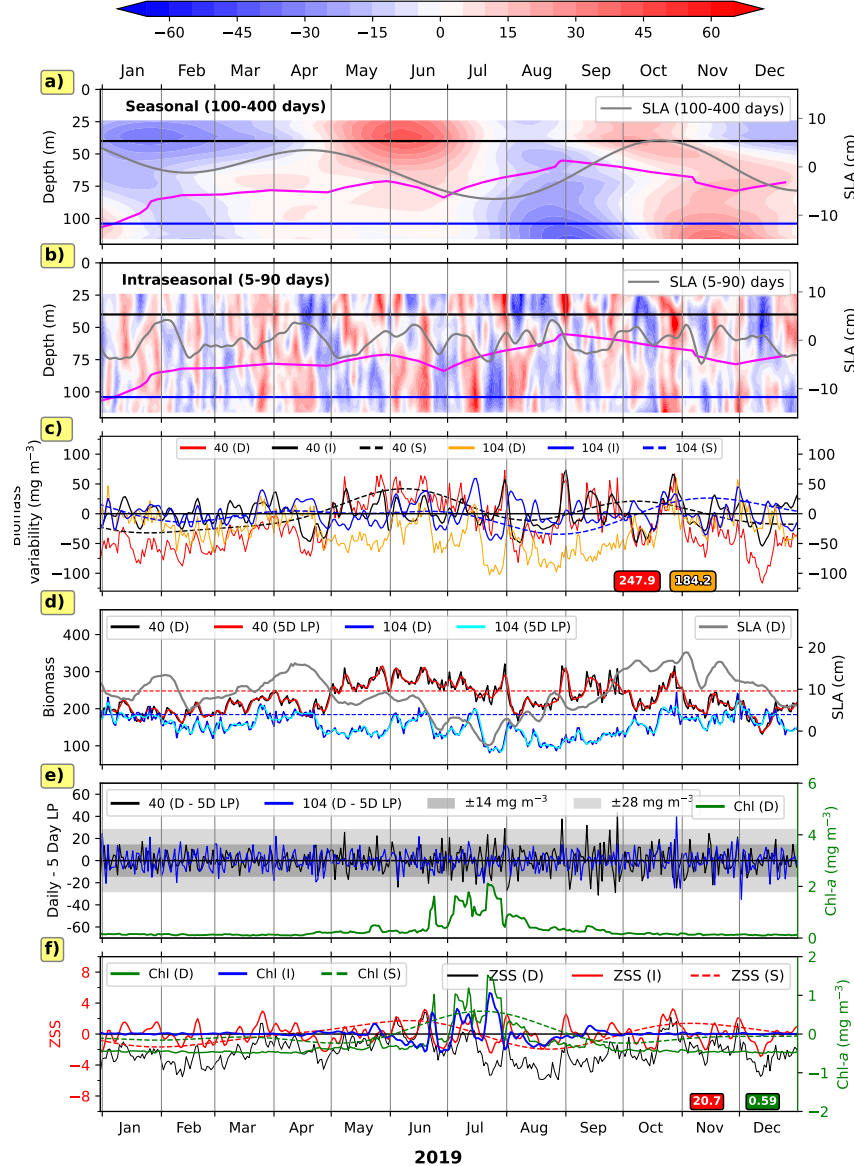


**Figure 11:** The figure shows a comparison of biomass variability ( $\text{mg m}^{-3}$ ) in the seasonal (100–400 days) and intraseasonal (5–90 days) bands off Kollam for the year 2019. For all panels, vertical grey lines separate the months. Panels (a) and (b) present time-depth plots of seasonal and intraseasonal biomass, respectively. Overlaid grey contours represent the corresponding SLA. Biomass at 40 m and 104 m depths is marked by black and blue horizontal lines. The magenta curves denote D175. Panel (c) shows the daily, intraseasonal, and seasonal biomass at 40 m and 104 m. The mean of the daily biomass time series for 40 m (red) and 104 m (orange) is indicated in the bottom right corner of this panel. Panel (d) compares daily SLA (grey) with daily and 5-day low-pass filtered biomass at 40 m and 104 m. Panel (e) illustrates the difference between daily and 5-day low-pass filtered biomass at both depths. Grey and light grey shaded regions denote the  $\pm 1$  SD and  $\pm 2$  SD bounds, respectively, derived from the backscatter-biomass relationship. Daily chl-*a* (green) is overlaid onto this panel. The persistent background fluctuations are observed irrespective of low or no variation in chl-*a*. The spikes, for example, in late August and September does not coincide with any specific peak in chl-*a*. The bottom panel (f) shows daily satellite chl-*a* and ZSS, and their variability in the intraseasonal and seasonal bands. See Figs. S4–S9 for detailed comparisons across variability bands for rest of the locations.